



Late Weichselian local ice dome configuration and chronology in Northwestern Svalbard: early thinning, late retreat



Endre F. Gjermundsen^{a,*}, Jason P. Briner^b, Naki Akçar^c, Otto Salvigsen^d, Peter Kubik^e, Niklas Gantert^a, Anne Hormes^a

^a Department of Arctic Geology, The University Centre in Svalbard, P.O.Box 156, 9171 Longyearbyen, Norway

^b Department of Geology, University at Buffalo, Buffalo, NY 14260, USA

^c Geologische Institut, UniBern, CH, Switzerland

^d Institute of Geosciences, University of Oslo, Norway

^e ETH Zürich, CH, Switzerland

ARTICLE INFO

Article history:

Received 20 September 2012

Received in revised form

7 April 2013

Accepted 9 April 2013

Available online 25 May 2013

Keywords:

Quaternary

Glacial geology

Cosmogenic exposure dating

¹⁰Be dating

Erratic boulders

Late Weichselian

Svalbard

Spitsbergen

Northwest Spitsbergen

The High Arctic

Svalbard Barents Sea Ice Sheet

ABSTRACT

The chronology and configuration of the Svalbard Barents Sea Ice Sheet (SBSIS) during the Late Weichselian (LW) are based on few and geographically scattered data. Thus, the timing and configuration of the SBSIS has been a subject of extensive debate. We present provenance data of erratic boulders and cosmogenic ¹⁰Be ages of bedrock and boulders from Northwest Spitsbergen (NWS), Svalbard to determine the thickness, configuration and chronology during the LW. We sampled bedrock and boulders of mountain summits and summit slopes, along with erratic boulders from coastal locations around NWS. We suggest that a local ice dome over central NWS during LW drained radially in all directions. Provenance data from erratic boulders from northern coastal lowland Reinsdyrflya suggest northeastward ice flow through Liefdefjorden. ¹⁰Be ages of high-elevation erratic boulders in central NWS (687–836 m above sea level) ranging from 18.3 ± 1.3 ka to 21.7 ± 1.4 ka, indicate that the centre of a local ice dome was at least 300 m thicker than at present. ¹⁰Be ages of all high-elevation erratics (>400 m above sea level, central and coastal locations) indicate the onset of ice dome thinning at 25–20 ka. ¹⁰Be ages from erratic boulders on Reinsdyrflya ranging from 11.1 ± 0.8 ka to 21.4 ± 1.7 ka, indicate an ice cover over the entire Reinsdyrflya during LW and a complete deglaciation prior to the Holocene, but apparently later than the thinning in the mountains. Lack of moraine deposits, but the preservation of beach terraces, suggest that the ice covering this peninsula possibly was cold-based and that Reinsdyrflya was part of an inter ice-stream area covered by slow-flowing ice, as opposed to the adjacent fjord, which possibly was filled by a fast-flowing ice stream. Despite the early thinning of the ice sheet (25–20 ka) we find a later timing of deglaciation of the fjords and the distal lowlands. Several bedrock samples (¹⁰Be) from vertical transects in the central mountains of NWS pre-date the LW, and suggest either ice free or pervasive cold-based ice conditions. Our reconstruction is aligned with the previously suggested hypothesis that a complex multi-dome ice-sheet-configuration occupied Svalbard and the Barents Sea during LW, with numerous drainage basins feeding fast ice streams, separated by slow flowing, possibly cold-based, inter ice-stream areas.

© 2013 Elsevier Ltd. All rights reserved.

1. Introduction

An understanding of the temporal and spatial changes of Late Quaternary ice sheets is fundamental to improved knowledge about their interactions with global and local sea level, climate change, climate/ice-sheet feedback mechanisms, and local and

regional sediment distributions. The marine-based SBSIS resembles the West Antarctic Ice Sheet, both being marine based and of similar size (Siegert et al., 2002), and reconstructions of the dynamics and subsequent disappearance of the SBSIS provide a potential analogue for understanding the response of the West Antarctic Ice Sheet to climate change.

At present, most of the studies regarding the SBSIS have been done by marine investigations (Elverhøi et al., 1995; Solheim et al., 1996; Svendsen et al., 2004; Ottesen and Dowdeswell, 2009; Dowdeswell et al., 2010), or carried out in coastal environments

* Corresponding author. Tel.: +47 79023360; fax: +47 79023301.
E-mail address: endreg@unis.no (E.F. Gjermundsen).

(Mangerud and Svendsen, 1992; Andersson et al., 1999; Alexanderson et al., 2011). Thickness estimates of SBSIS are based on isostasy (Forman et al., 2004), and few studies have investigated high-elevation, inland areas of the Svalbard Archipelago to investigate ice sheet thickness (Landvik et al., 2003; Hormes et al., 2011; Landvik et al., 2013). However, many characteristics about the SBSIS remain unsolved, such as ice sheet thickness, the timing of interior thinning, the chronology and pattern of deglaciation, and its complex multidome configuration. Cosmogenic nuclide exposure dating is a tool that potentially can address remaining uncertainties. This research focuses on the northwestern SBSIS; our study area encompasses ~20% of Spitsbergen (Fig. 1).

2. Background

The onset of major glaciation of the Barents Sea is based on the intensification of IRD pulses at ~3.2 to 2.7 Ma on the eastern side of the Norwegian–Greenland Sea, including the Barents Sea margin (Thiede et al., 1998). This was recently confirmed by Knies et al. (2009), who revised the chronostratigraphy using a compilation of borehole data from the Barents Sea continental margin. During the Quaternary, ice sheets in the Arctic have grown and advanced across the high-latitude continental shelves to reach the shelf edge a number of times (e.g., Elverhøi et al., 1998; Ottesen and Dowdeswell, 2009). During the Weichselian alone, three major glacial advances have been identified on Spitsbergen (Mangerud et al., 1998).

The extent of the SBSIS during LW has been a subject of debate (Hormes et al., submitted for publication). Ice sheet reconstructions range from limited ice (Boulton, 1979; Troitsky et al., 1979; Boulton et al., 1982; Forman and Miller, 1984) to a large continuous ice sheet over Svalbard and the entire Barents and Kara seas and confluent with the Fennoscandian Ice Sheet (Schytt et al., 1968; Andersen, 1981; Mangerud and Svendsen, 1992; Mangerud et al., 1992; Grosswald and Hughes, 1995; Landvik et al., 1998; Svendsen et al., 2004; Vorren et al., 2010). Currently, there is a general consensus that the SBSIS reached the shelf edge in the west and north, and that the eastern margin reached the northwestern part of the Kara Sea, during the LW. Recent studies, particularly of sea floor morphology, have led to a better understanding SBSIS dynamics along its western margin (Elverhøi et al., 1998; Landvik et al., 2003, 2005; Ottesen et al., 2007; Ottesen and Dowdeswell, 2009; Dowdeswell et al., 2010; Hogan et al., 2010; Vorren et al., 2010). The SBSIS began to grow at ~32 ka, achieved a maximum phase ~24 ka (Jessen et al., 2010), and began to retreat from its maximum position ~21 ka (Jessen et al., 2010). On Reinsdyrflya (Fig. 1), a flat and elongated coastal lowland in the northeastern corner of our study area, Salvigsen and Österholm (1982) mapped glacial striae, suggesting it had been covered by ice. However, due to undisturbed pre-LW raised beach terraces and the lack of LW glacial sediments, Salvigsen and Österholm (1982) concluded that Reinsdyrflya was not overridden during the LW.

The recent depiction of ice configuration involves individual ice domes and fast flowing ice streams, separated by slow flowing, cold-based inter ice-stream areas during peak glacial advances (Landvik et al., 2005; Ottesen and Dowdeswell, 2009; Alexanderson et al., 2011; Hormes et al., 2011). However, there remain few data on the vertical extent of the LW ice sheet. Based on ¹⁰Be analyses of bedrock and boulders on Amsterdamøya and Danskøya (Fig. 1), Landvik et al. (2003) suggested that the summits of these islands in the northwestern corner of the archipelago had been ice free for >80 ka, and that the adjacent fjords were filled with low gradient outlet glaciers or ice streams during LW. In a more recent work, Landvik et al. (2013) used the same approach to map the ice sheet elevation in Trongdalen, on

Mitrahølvøya and on the northern parts of Prins Karls Forland (Fig. 1), in order to better understand the paleodynamics of the LW ice sheet in this coastal area. They suggested that ice reached elevations of >470 m above sea level (a.s.l.) at Prins Karls Forland and possibly >313 m a.s.l. at Mitrahølvøya during LW. Glacial striae found up to ~80 m a.s.l. showed that warm-based conditions had existed locally and/or temporarily even though age difference between ¹⁰Be ages of bedrock and boulders suggested limited glacial erosion during the LW. They also concluded that the glacier surface in inter ice-stream areas represented a topographic high compared to the elevations of active ice streams that drained Isfjorden and Kongsfjorden. Another recent study, from Nordaustlandet (Fig. 1), concluded that the warm-based part of the LW ice sheet was restricted to the fjords and lowlands below 200–230 m a.s.l. (Hormes et al., 2011). In this study, bedrock and boulder samples also yielded different ages, indicating a complex glacial and exposure history.

3. Study site and geology

NWS (79°–80° N; Fig. 1) is occupied by interconnected ice-fields, so-called glaciers of Spitsbergen type (Hagen et al., 1993). Spectacular contrasts exist from the large strandflats in the south (Mitrahølvøya) and north (Reinsdyrflya) to steep mountains in the interior that feed glaciers terminating the sea (Fig. 2). Today, more than 60% of NWS is covered by glaciers (König et al., 2011), including large ice streams such as Monacobreen, the largest ice stream with an area of ~400 km², and Lilliehöökreen, the second largest ice stream with an area of ~250 km². NWS has a total glacier cover of almost 2000 km² and a climatic equilibrium line of ~300 m a.s.l. (Hagen et al., 1993). Most of the glaciers on Svalbard have retreated significantly since the Little Ice Age (Nuth et al., 2007). Many glaciers in the area are likely surge-type glaciers; Chaveauxbreen, on Vasahølvøya (Fig. 1), surged as recently as 1990 (Sund et al., 2009). Mountain summits are >1000 m a.s.l. with the highest being Kongen, in the southern part of the area at 1458 m a.s.l. In the northern part of the area, Jäderinfjellet and Auriviliusfjellet reach >1100 and Munken (1205 m a.s.l.) is the highest peak here (Fig. 1). The LW marine limit at Gråhøken, the northern tip of André Land, is 80 m a.s.l. (Brückner et al., 2002). The marine limit on the southern fringe of Reinsdyrflya (Sørdalsflya) is 25 m a.s.l. (Salvigsen and Österholm, 1982; Lehman, 1989), whereas at the head of Liefdefjorden it reaches only 4–5 m a.s.l. The marine limit on Amsterdamøya and Danskøya is 0 m a.s.l. (Salvigsen, 1979); thus, the regional marine limit rises from west to east. On the southwestern part of Mitrahølvøya, Forman (1990) documented a marine limit of 20 m a.s.l., and on the eastern part of the peninsula it is 25 m a.s.l. Landvik et al. (2013), however, observed marine limit elevations of 32 and 39 m a.s.l. in the Trongdalen area (Fig. 1).

NWS is dominated by migmatitic para- and orthogneisses and Caledonian granitoids from the mid-Silurian Caledonian orogeny (430 ma; Ohta et al., 2002). North of Kongsfjorden and west of Woodfjorden, pre-Devonian crystalline bedrock of the Caledonian orogeny is exposed. The Caledonian Orogen was separated along sinistral transtensional/transpressional faults into different terrains (Gee et al., 2008). Precambrian migmatites and gneisses are intruded by Caledonian red monzogranite (Ohta et al., 2002), which is named Hornemantoppen Granite after the central peak in the area (Fig. 1). Because of its characteristic reddish colour and coarse grained nature, erratics of Hornemantoppen Granite are easy to distinguish in the field, and they give unambiguous information about former ice flow paths in the area. Salvigsen and Österholm (1982) reported a frequent distribution of Hornemantoppen Granite erratics on Danskøya and at 400 m a.s.l. on Amsterdamøya.

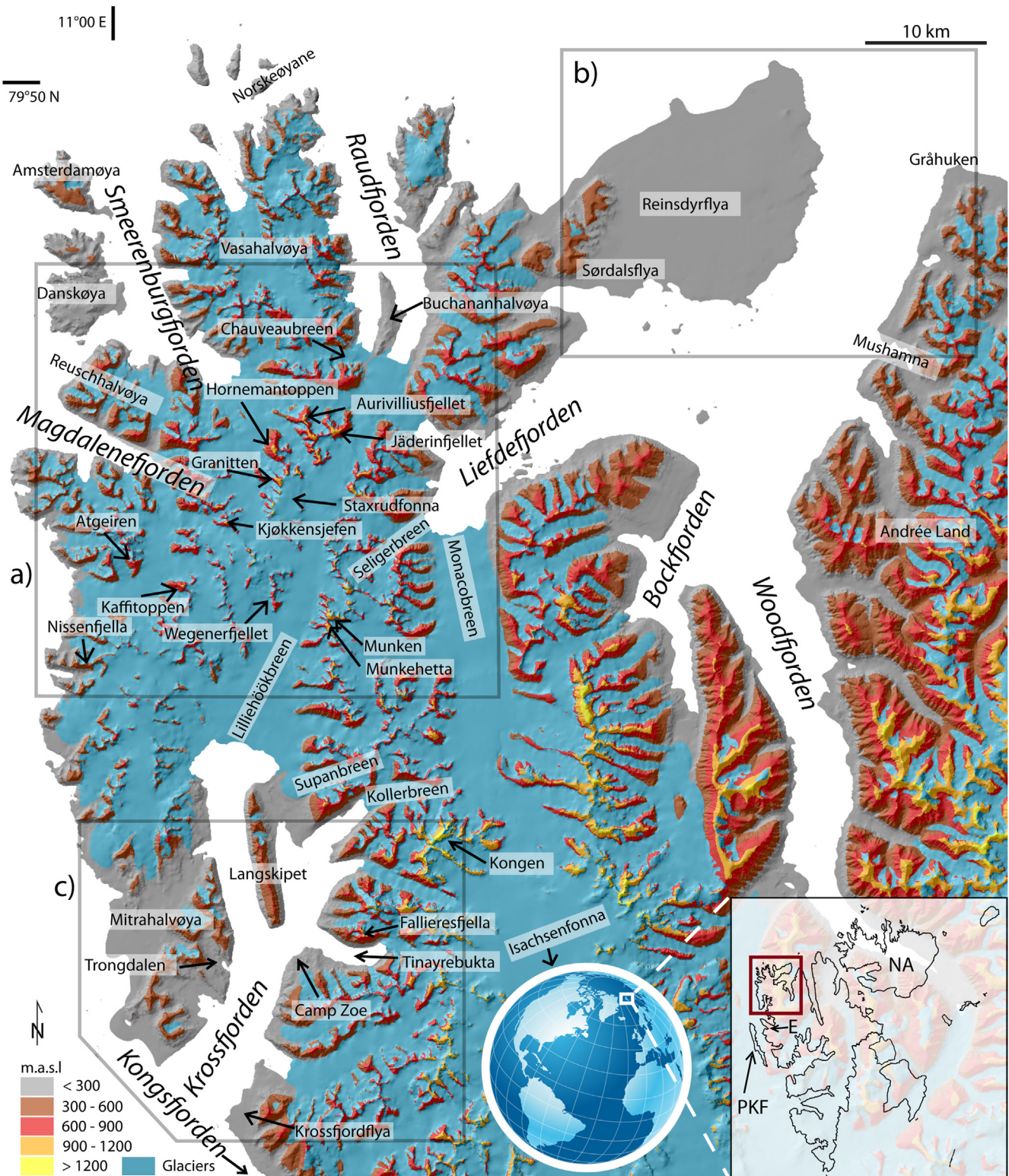


Fig. 1. Study area Northwest Spitsbergen on the Svalbard archipelago. The figure shows the topography in the area and a digital elevation model from the Norwegian Polar Institute is used as a base. Everything in blue marks the extension of today's glaciers and is from an unpublished glacier inventory from recent satellite data. Abbreviation on Svalbard map inset: PKF = Prins Karls Forland, NA = Nordaustlandet, E = Engelsbukta. The windows a, b, c, show the locations of the three close up views in Fig. 3. (For interpretation of the references to colour in this figure legend, the reader is referred to the web version of this article.)

They also found one large block on Indre Norskøya, farther out in the Smeerenburgfjord (Fig. 1). Hornemantoppen Granite erratics also have been transported to the shores of Liefdefjorden and to Reinsdyrflya. Most of them were found below 100 m a.s.l. (Salvisgen

and Österholm, 1982), but some were found at >500 m a.s.l. west of Reinsdyrflya. The distribution of Hornemantoppen Granite erratics showed that glaciers have transported rocks of this type from the batholith towards the west, north and east. However, they did not

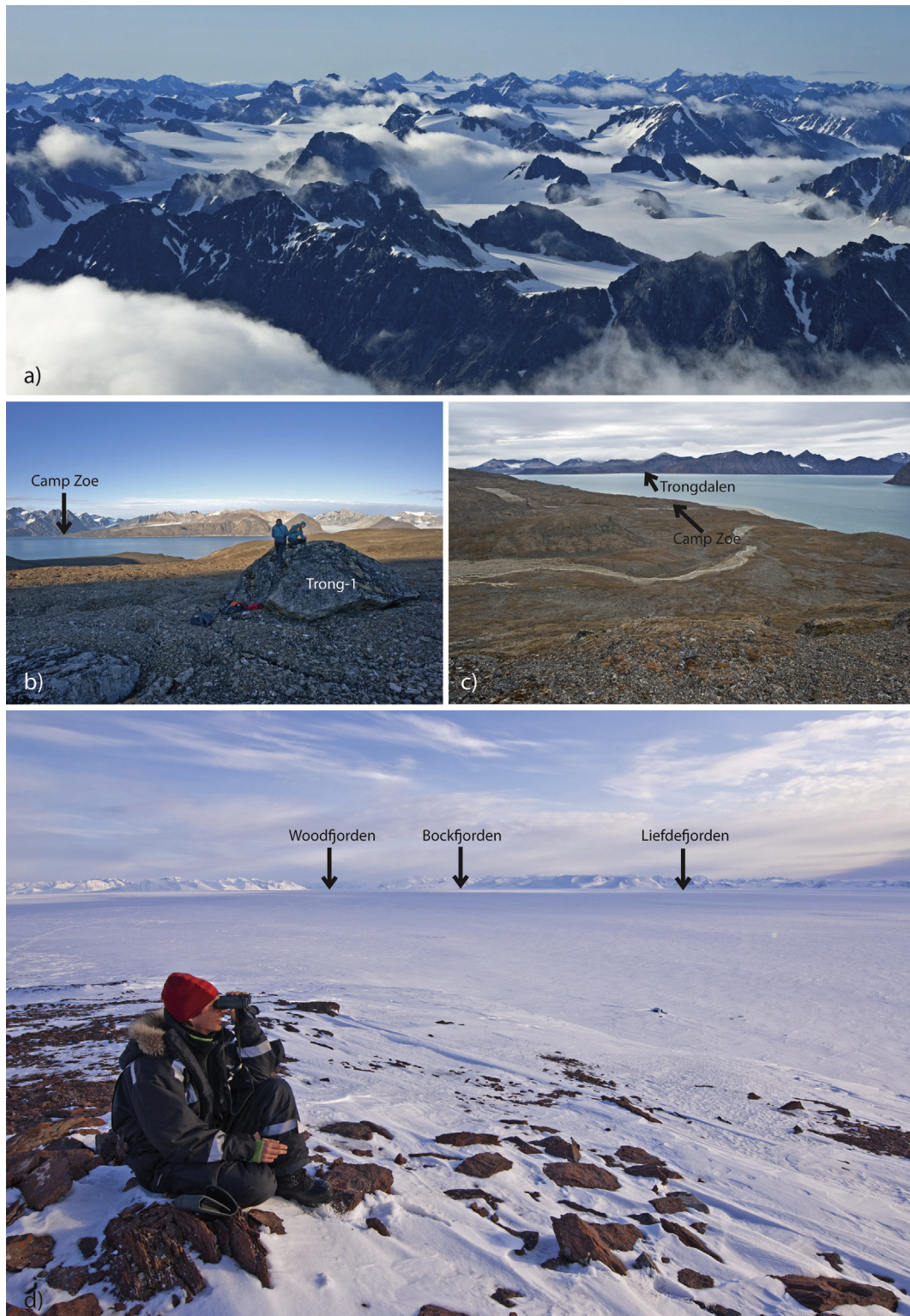


Fig. 2. Illustrations of landscape types in the field area. a) alpine landscape (view from the shoulder of Kongen, looking north), b) and c) subalpine terrain in Krossfjorden d) flat, low relief terrain on Reinsdyrflya.

find Hornemantoppen Granite erratics east of Woodfjorden. The southern part of the northwestern terrain is composed of schist and marble close to Kongsfjorden (Gee et al., 2008). Our study area is separated along the N-trending Raudfjorden Fault from the early Devonian fluvial sandstones and conglomerates. West of the

Raudfjorden Fault, the Schmeerenburg Complex of schist, gneiss and migmatite is abundant. East of this fault the bedrock is composed of Devonian Old Red sandstone overlying the crystalline complex consisting of pelitic schist, amphibolite, gneiss and marble.

4. Methodology

4.1. Field data collection and procedures

Samples from erratic boulders were collected for ^{10}Be dating from Reinsdyrflya and Mitrahålvøya in the northeastern and southern NWS, respectively, as well as from the eastern side of Krossfjorden and Woodfjorden (Figs. 1 and 3). All these boulders, except the one sampled on Lanskipet (Fig. 9g), were >1.5 m high and most of them were >10 m³ (Fig. 4). In order to investigate the thickness of the ice, samples from summits and high-elevation ridges were also collected. By conducting the majority of the field work during the winter months, we avoided sampling sites that were heavily affected by snow cover. Erratic boulders and bedrock surfaces with very little snow were chosen for sampling assuming that these windswept sites were windswept not only during our field campaigns, but during all seasons and during most years.

Samples were collected using hammer and chisel, and we followed standard sampling strategies (Ivy-Ochs et al., 1996; Akcar et al., 2011). Sample thickness was typically 3–5 cm and a few thicker samples were cut in the lab to 5 cm. Position and altitude of each site were recorded with a barometrically corrected GPS and some were later corrected to a digital elevation model (DEM) from the Norwegian Polar Institute (spatial resolution 20 m) for validation purposes. In the steep and alpine topography of central NWS even a small error in GPS position could give a larger spatial error compared to flatter terrain. Topographic shielding was either measured using an inclinometer and calculated using topographic scaling factors (Dunne et al., 1999) or obtained from an automated technique using a DEM in ArcMap (Codilean, 2006). The topographic shielding and strike and dip corrections result in a 0.3–6% decrease in the ^{10}Be production rate except “Kjoek-2,” which was collected from a vertical wall and therefore has a correction factor of 0.5 (Table 1).

4.2. Sample preparation, ^{10}Be measurements and exposure age calculation

After crushing and sieving, samples were split into magnetic and non-magnetic fractions with a Frantz magnetic separator; the non-magnetic fraction was purified with respect to quartz (Kohl and Nishiizumi, 1992; Ivy-Ochs et al., 1996; Akçar, 2006). The ^{10}Be isotope extraction was carried out in batches of five (four samples and one process blank). Samples were spiked with a Be carrier with a $^{10}\text{Be}/^9\text{Be}$ ratio of $(2.2 \pm 0.1) \times 10^{-14}$. The purified quartz samples were processed at the Surface Exposure Dating Laboratory of the University of Bern and measured for $^{10}\text{Be}/^9\text{Be}$ at the ETH/PSI tandem AMS facility in Zürich (Kubik and Christl, 2010). The measurements have been normalized to the in-house standard S555 and S2007N for $^{10}\text{Be}/^9\text{Be}$. ^{10}Be concentrations of the samples, which are measured with in-house standard S555 prior to April 2010, have been re-normalized to the 07KNSTD standard by applying conversion factors of 0.9124 (Kubik and Christl, 2010). For ^{10}Be age calculations, a production rate of 3.96 ± 0.16 atoms $\text{g}^{-1} \text{SiO}_2$ (spallogenic production only) was used from the regional production calibration in northern Norway (Fenton et al., 2011). Altitude/latitude scaling of the production rates was made according to (Stone, 2000) with muon contributions of 2.2%. Changes in palaeomagnetic intensity and polar wander were not taken into account because their effects on the nuclide production were smaller than 1% at this latitude (Masarik et al., 2001). Depth correction was made using an apparent exponential attenuation length of 160 g cm^{-2} (Masarik and Reedy, 1995). We used a rock density of 2.65 g cm^{-3} (Table 1). No correction is applied for shielding by snow cover. The post-glacial emergence for NWS is 25 m for southern Reinsdyrflya (Salvigsen and Österholm, 1982; Lehman, 1989) and 20 m for southwestern Mitrahålvøya (Forman, 1990). The isostatic rebound was rapid between 13 and 10 ka and present-day shorelines are less than 5 m

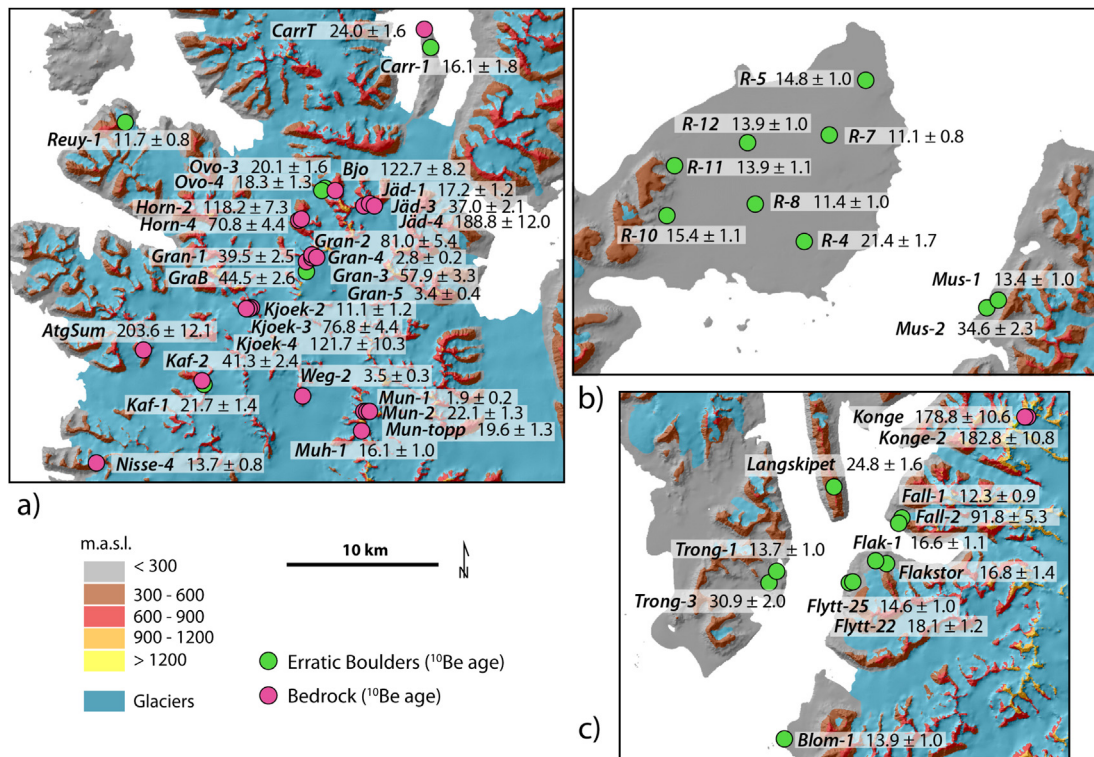


Fig. 3. All our analysed boulder and bedrock samples from Northwest Spitsbergen including their respective ^{10}Be ages and external uncertainties. Window a) show the central, high-elevation area, whereas b) shows Reinsdyrflya and c) the Krossfjorden area.



Fig. 4. Illustrations of sampling sites. a) and b) the summit of Atgeiren (the “AtgSum” site), c) large erratic boulder in Krossfjorden with view towards Lanskipet (the “Flakstor” sample), d) sampling of an erratic boulder on Reinsdyrflya, e) erratic boulder of syntectonic metamorphosed light grey granite deposited on Devonian sandstone on Reinsdyrflya (R-5; hat for scale), f) the walls of Kongen, syntectonic metamorphosed light grey granite, g) sampling an erratic boulder in Krossfjorden (Fall 1), h) sampling a boulder in the central Northwest Spitsbergen (the “GraB” sample).

higher than they were at 10 ka. Because of the minimal Holocene uplift in this area, ^{10}Be ages were not corrected for uplift. ^{10}Be ages and their external uncertainties were calculated using the CRONUS online exposure age calculator (Balco et al., 2008; Table 1).

4.3. Provenance

Lithologies of erratic boulders were investigated to define their most likely source area and subsequently to reconstruct ice flow

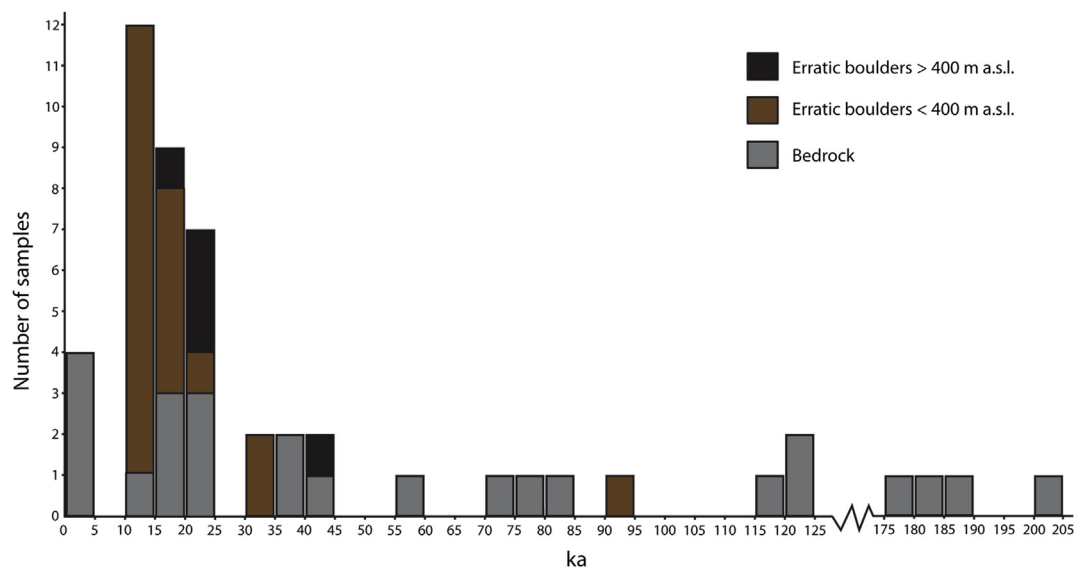


Fig. 5. Frequency histogram of the sample, showing the age distribution of our 50 analysed samples.

direction (Fig. 4). However, reconstruction of ice flow direction can at best be the net transport direction of the erratics. Thin sections were made for select samples at the Department of Geology, University of Tromsø. Erratic boulders deposited on mountain ridges, plateaus or summits were sought provide insight into the minimum surface elevation of the LW ice sheet in the area. In addition, boulder lithology was also used to define drift boundaries and provide insight into ice sheet thermal regime.

5. Results

5.1. Erratics

We produce 25 ^{10}Be ages from erratic boulders in NWS (Table 1; Figs. 3, 5 and 6). In the northeastern portion of NWS, on Reinsdyrfløya, seven ^{10}Be ages from erratic boulders range from 11.1 ± 0.8 to 21.4 ± 1.7 ka. Nearby at Mushamna, on the east side of Woodfjorden, two boulders yield ages of 34.6 ± 2.3 and 13.4 ± 1.0 ka. On Buchanahalvøya, in Raudfjorden, in the northern part of the study area, one erratic boulder at 110 m a.s.l. (Carr-1) yield a ^{10}Be age of 16.1 ± 1.8 ka.

In central NWS, ^{10}Be ages from three erratic boulders from mountain ridges (>680 m a.s.l.) indicate past ice flow directions and the timing of ice sheet thinning. Ovo-3 (687 m a.s.l.) and Ovo-4 (730 m a.s.l.), both on the shoulder of Aurivilliusfjellet, are 20.1 ± 1.6 and 18.3 ± 1.3 ka, respectively. These two erratics are located >250 m higher than the local glacier surface in the area today, (Fig. 7), and one boulder on Kaffitoppen (Kaf-1; 21.7 \pm 1.4 ka) at 836 m a.s.l. is >300 m above today's glacier surface encircling the mountain (Fig. 8). In the western portion of NWS, on Reuschhalvøya (Fig. 1), near Danskøya and Amsterdamøya, an erratic boulder at 300 m a.s.l. (Reuy-1) yields a ^{10}Be age of 11.7 ± 0.8 ka. One erratic boulder on a mountain shoulder west of Staxrudfonna (Fig. 1), GraB, at 855 m a.s.l., gives a ^{10}Be age of 44.5 ± 2.6 ka.

In the southern portion of NWS, nine boulders from Krossfjorden, including two from Mitrahøya (Fig. 1), range from 10 to 30 ka (Fig. 5), after excluding one old outlier (Fall-2; 91.8 ± 5.3 ka). An erratic at 611 m a.s.l. on Langskipet, a high-elevation peninsula above Krossfjorden, yields a ^{10}Be age of 24.8 ± 1.6 ka (Fig. 9).

5.2. Bedrock

We produce 25 ^{10}Be ages from bedrock in the central, high-elevation portion of NWS (Table 1). The bedrock ^{10}Be ages range from 1.9 ± 0.2 to 203.6 ± 12.1 ka. 19 of the 25 ^{10}Be ages from bedrock are between 15 and 205 ka (Fig. 5). In general, the oldest ages are from the highest elevations, as illustrated from Jäderinfjellet. For example, sample Jäd-4, from the summit of Jäderinfjellet (188.8 ± 12.0 ka) has a similar age as the two bedrock samples from Kongen (178.8 ± 10.6 and 182.8 ± 10.8 ka). Sample Jäd-3, collected 120 m lower than the summit of Jäderinfjellet, is 37.0 ± 2.1 ka. Our lowermost bedrock sample from Jäderinfjellet (Jäd-1; 893 m a.s.l.) is from just above today's glacier surface (~700 m a.s.l.) and yields an age of 17.2 ± 1.2 ka. The rest of our summit transects show similar trends, with the oldest ages at the highest elevations and decreasing ages towards lower elevations. Additionally, one very old ^{10}Be age from the summit of Atgeiren (930 m a.s.l.) in the western part of NWS is 203.6 ± 12.1 ka (Fig. 4).

5.3. Lithologies

Reinsdyrfløya is well-suited for provenance studies because it is entirely composed of Devonian red sandstones and all far-travelled boulders can be clearly identified. Here, we found lithologies sourced in the central NWS, >30 km to the southwest. The analysed samples were migmatite or syntectonic granite (Table 1). One large Hornemantoppen Granite erratic was also found (Fig. 6).

Hornemantoppen Granite was also found on Reuschhalvøya (Figs. 1 and 6). The boulders sampled for ^{10}Be dating in Krossfjorden consisted of migmatite, gneiss and syntectonic granite; some of them located >15 km away from their source.

6. Interpretation and discussion

6.1. Timing of deglaciation

6.1.1. Interior thinning

Our high-elevation erratics indicate that the ice sheet started to thin as early as 25–20 ka. The erratics from central NWS range between 18.3 ± 1.3 and 21.7 ± 1.4 ka (excluding the outlier GraB at 44.5 ± 2.6 ka) and the erratic from Langskipet (24.8 ± 1.6 ka, 611 m

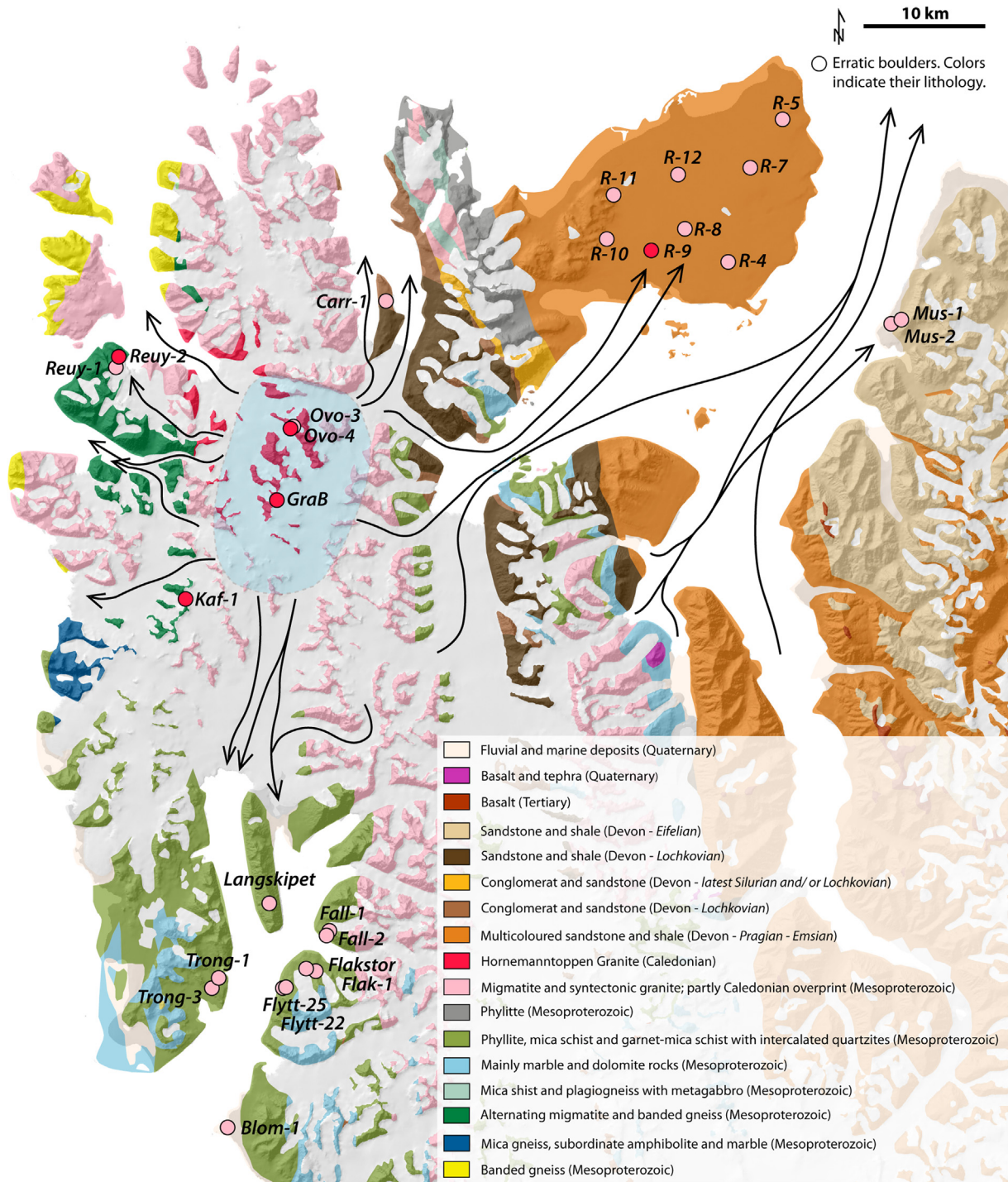


Fig. 6. Geological map of Northwest Spitsbergen with location of our suggested ice dome and its drainage directions. The geological map is modified from Dallmann et al. (2002) and is draped over a hillshade made from a digital elevation model from the Norwegian Polar Institute.

a.s.l.; Fig. 9) indicate that thinning initiated relatively early during the LW.

6.1.2. Distal retreat

The average ¹⁰Be age of 14.6 ± 3.4 ka from the erratic boulders on Reinsdyrflya indicate the presence of ice on the entire peninsula during LW and deglaciation apparently after initial thinning in the central NWS mountains. The age of 13.4 ± 1.0 ka from the eastern side of Woodfjorden supports the age from Reinsdyrflya, and

supports deglaciation of outer Woodfjorden at this time. Similarly, the age of 13.7 ± 0.8 ka from the slope of Nissenfjella, in the western extremity of our area suggests a similar timing of deglaciation there. In the Krossfjorden area, our sample Trong-1 (13.7 ± 1.0 ka) matches the ages of the samples recently reported by Landvik et al. (2013) in the same area who provided two boulders and one cobble averaging 13.9 ± 1.2. However, our erratic boulder ages on the eastern side of the fjord are slightly older (12–18 ka).

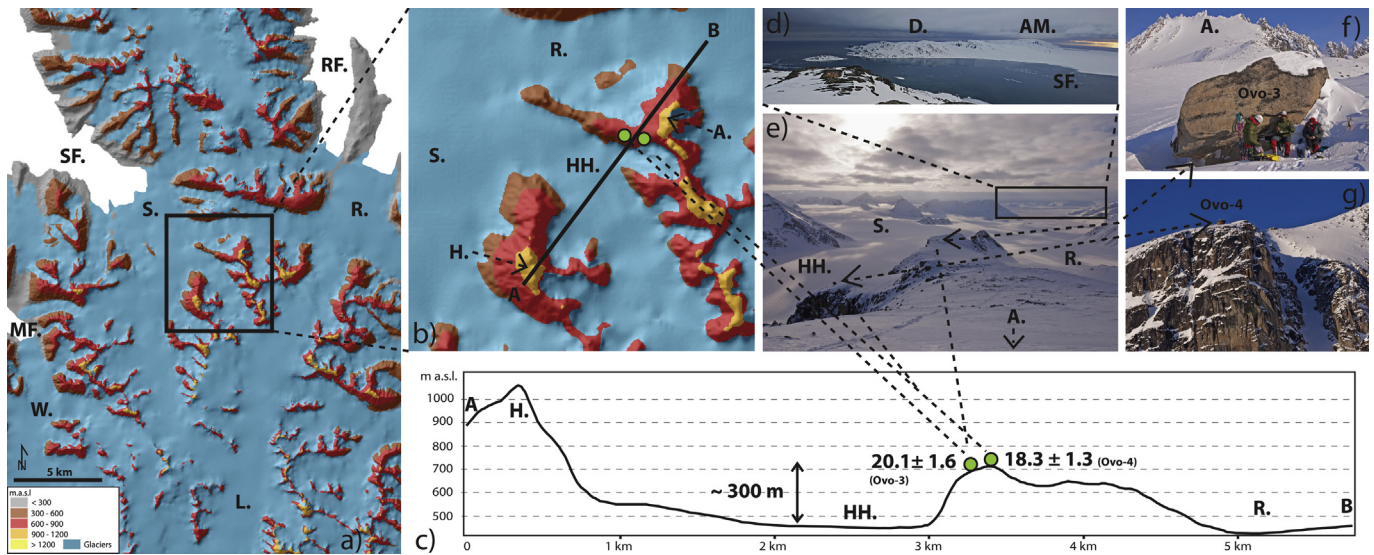


Fig. 7. Erratic boulder samples on Aurivilliusfjellet in central Northwest Spitsbergen. a) Overview of area, b) close up view of the sampling area with location of profile given in c), c) profile shown in b) with locations of samples, d) zoomed in view as given in e) showing the two islands west of Smeerenburgfjorden, e) photo of sampling sites (arrows indicate location of samples), f) close up view of “Ovo-3”, g) location of the “Ovo-4” sample, seen from below. Abbreviations from left to right: MF = Magdalenefjorden, W = Waggonwaybreen, SF = Smeerenburgfjorden, S = Smeerenburgbreen, L = Lilliehøokbreen, RF = Raudfjorden, R = Raudfjordbreen, H = Hornemantoppen (1092 m a.s.l.), R = Rakbreen, HH = Hans Henrikbreen, A = Aurivilliusfjellet (north summit, 1072 m a.s.l.), D = Danskøya, AM = Amsterdamøya.

Taken together, we suggest that the distal lowlands around NWS were deglaciated ca 15–14 ka. However, there are some complications to this interpretation. On the eastern side of Krossfjorden, the older erratics ages of 15–18 ka are difficult to interpret. Landvik et al. (2013) suggested that local ice was dominating on Mitrahalvøya at the end of LW, leaving ice in the area for longer than the period occupied by the main ice sheet. This could explain the

difference in ages on the two sides of Krossfjorden, but would not explain the prevalence of 14–15 ka ages elsewhere around NWS.

6.1.3. Outliers

Several studies have shown that bedrock exposure ages may suffer from nuclide inheritance due to overriding by non-erosive ice (Stroeven et al., 2002; Briner et al., 2005, 2006; Li et al., 2005;

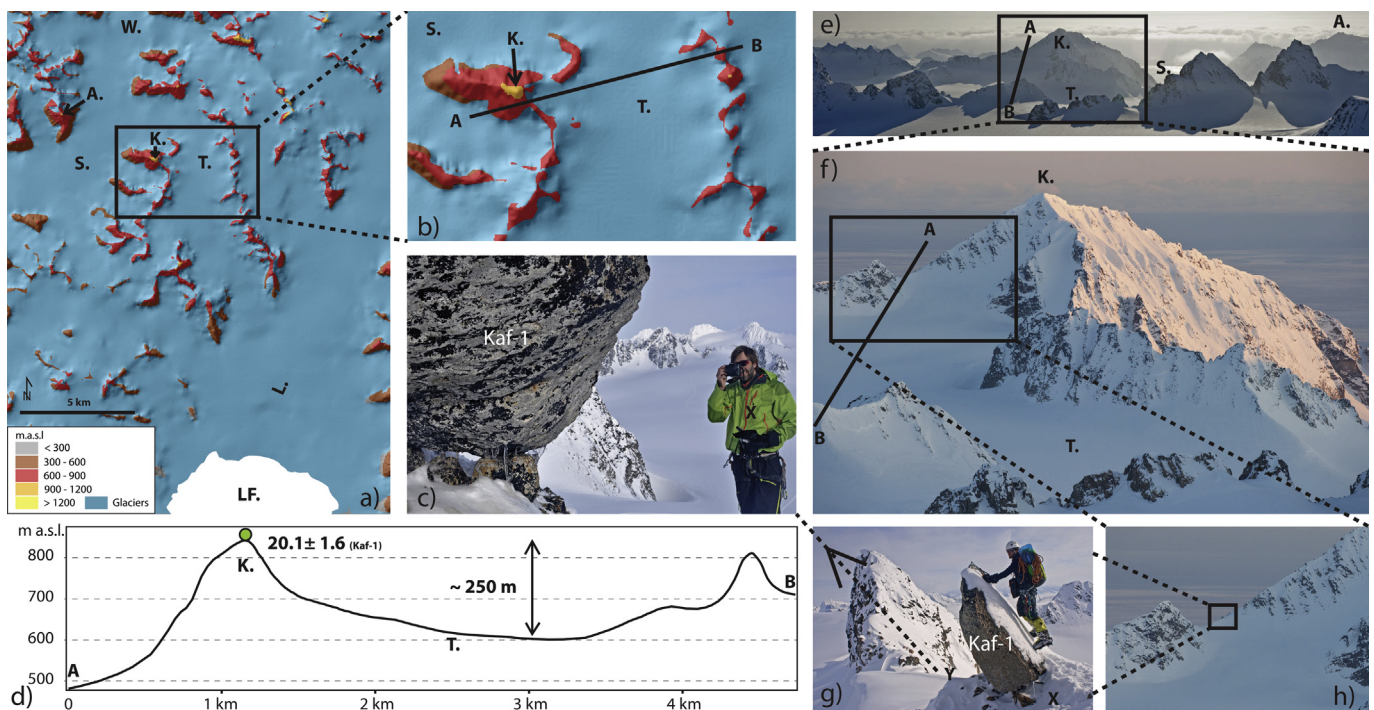


Fig. 8. Erratic boulder on Kaffitoppen. a) Overview of the area, b) close-up view of the sampling area with the profile given in d), c) close up view of the “Kaf-1” sample, illustrating that it is a perched boulder. Location of person, -X, is given in g), d) profile going through our sampling site and the glacier below. Location of profile is given in b), e), and f). The arrows in the profile indicate the minimum surface lowering since Late Weichselian, e) far distance view of Kaffitoppen (974 m a.s.l.) seen from east towards west, f) closer view of Kaffitoppen, g) close up look of the perched boulder. Y marks the position where the photograph in c) is taken, h) zoomed in view of the ridge where the perched boulder is found, showing the boulder as a very small dot. Abbreviations from left to right: S = Sjettebreen, A = Atgeiren, W = Waggonwaybreen, K = Kaffitoppen, T = Tjalkbreen, LF = Lilliehøokfjorden, L = Lilliehøokbreen.

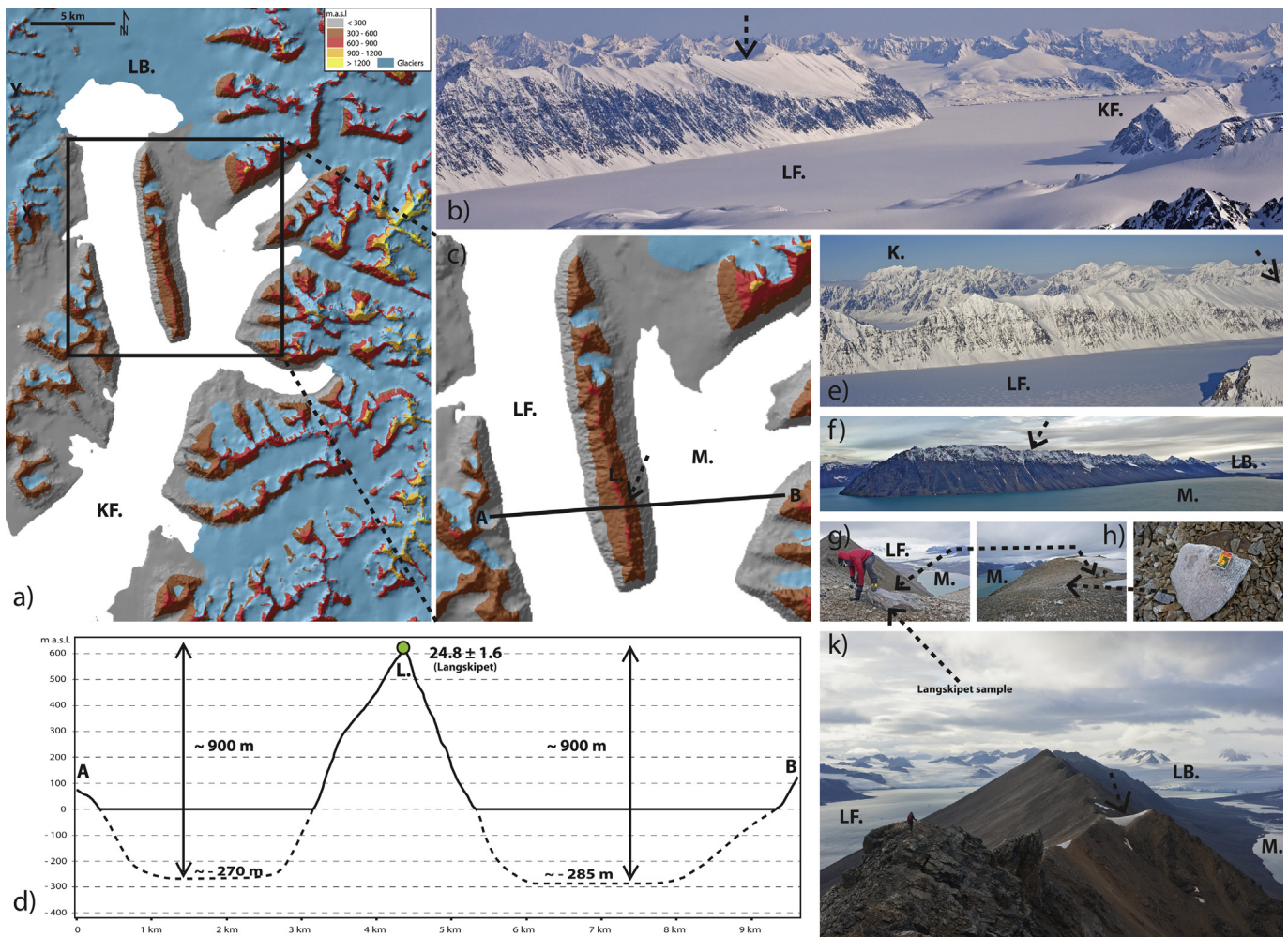


Fig. 9. Erratic boulder on Langskipet in Krossfjorden. a) Overview of the area, b) photo of the southern part of Langskipet taken from northwest (position X in a)), arrow indicate sample location, c) zoomed in view of Langskipet showing the location of the profile in given in d), d) profile through our sampling site on Langskipet as indicated in figure c). The arrows indicate the minimum ice thickness in Krossfjorden during LW in order to deposit the boulder on the summit ridge. e) photo of the northwestern part of Langskipet taken from northwest (position Y in a), f) photo of the entire Langskipet as seen from southeast (position Z in a)), g) taking our sample, h) photo of the sampling site showing the shape of the small sampling basin and the positions of our analysed sample in addition to the small erratic gneiss which we did not analyse, k) the summit ridge of Langskipet seen from south to north. The arrow on the figures points to the sampling site. Abbreviations from left to right: KF = Krossfjorden, LF = Lilliehöökfjorden, LB = Lilliehöökbrean, M = Möllerfjorden.

Phillips et al., 2006; Goehring et al., 2008). In these studies, LW erratics were deposited on pre-LW surfaces, indicating that even though subglacial erosion was limited at the ice/bedrock interface, lateral flow with entrained erratics occurred in the overlying ice mass. In a recent study from Nordaustlandet, Hormes et al. (2011) showed that most bedrock samples and even erratics contained nuclide inheritance, which was thought to be due to limited subglacial erosion along the northern margin of SBSIS.

Sample Fall-2, on the east side of Krossfjorden, with an age of 91.8 ± 5.3 ka, is clearly an outlier (Fig. 5) because it is located just a few hundred metre away from Fall-1, which is 12.3 ± 0.9 and is consistent with our ^{10}Be ages elsewhere in NWS. Sample GraB in the centre of NWS (44.5 ka) is also likely an outlier (Fig. 5) because it is less than ~ 100 – 150 m above the present glacier surface and it is unlikely that this not was covered by ice during the LW. The ice at this elevation (855 m a.s.l.) was possibly cold-based and non-erosive. This is also suggested in the work of Gjermundsen et al. (submitted for publication). On the other hand, given the LW ages from some of our high-elevation boulders from central NWS (Ovo 3, -4; Kaf-1; Fig. 5), along with the relatively long transport distance for the analysed Langskipet boulder, we suggest that these do not

contain inheritance. Assuming that the deglaciation of Mushamna on the eastern side of Woodfjorden is similar to the deglaciation age of Reinsdyrflya (average 14.6 ± 1.1 ka), we interpret the older age (34.6 ± 2.3 ka) as an outlier due to inheritance (Fig. 5). In addition, our other ^{10}Be age from Trongdalen (Trong-3, 30.9 ± 2.0 ka) is an outlier and likely subject to inheritance (Fig. 5).

A few bedrock samples are clearly young outliers. These samples are Mun-1 (1.9 ± 0.2 ka), Weg-2 (3.5 ± 0.3 ka), Gran-4 (2.8 ± 0.2 ka) and Gran-5 (3.4 ± 0.4 ka) (Fig. 5). These four samples are possibly from rock surfaces that only recently were exposed due to rock-fall, although no obvious indication of this was observed in field.

6.1.4. Comparison with other studies

Radiocarbon ages of marine shells on raised beach terraces in the vicinity of Mushamna yield ages younger than our ^{10}Be ages for deglaciation of the coastal areas (Bruckner and Schellmann, 2003). One sample from Mushamna is ~ 11.5 cal ka BP (all ^{14}C ages are reported in calibrated years using standard marine reservoir correction; $\Delta R = 40$; Mangerud et al., 2006), and several samples around Vårfluesjøen (~ 7 km north of Mushamna) lie between ~ 12.5 and 13.0 cal ka BP. It is thought that the deglaciation of

Table 1
Numbers inserted into the Cronus Earth calculator, along with calculated sample ages and lithological information. Inputs to the Cronus Earth calculator not found in the table are given in the footnote.

Sample	Mountain/or area	¹⁰ Be exposure age (with external uncertainty)	Elevation (m a.s.l.)	Lithology	Latitude	Longitude	Shielding correction	¹⁰ Be concentration (atoms/g ⁻¹)	Uncertainty of ⁸⁰ Be (atoms/g ⁻¹)
Boulders									
Ovo-3	Aurivilliusfjellet	20.1 ± 1.6	687	Syntectonic, light grey granite, gneissic	79.60131	11.78664	0.999647	165296	10082
Ovo-4	Aurivilliusfjellet	18.3 ± 1.3	730	Hornemantoppen granite	79.59878	11.81672	0.999765	156942	8239
R-4	Reinsdyrflya	21.4 ± 1.7	85	Syntectonic, light grey granite, gneissic	79.73753	13.61424	1.0	96288	5781
R-5	Reinsdyrflya	14.8 ± 1.0	97	Syntectonic, light grey granite, gneissic	79.83747	13.79804	1.0	74140	3162
R-7	Reinsdyrflya	11.1 ± 0.8	69	Migmatite	79.80773	13.65270	1.0	53987	2538
R-8	Reinsdyrflya	11.4 ± 1.0	75	Syntectonic, light grey granite, gneissic	79.75640	13.40483	1.0	50947	3717
R-10	Reinsdyrflya	15.4 ± 1.1	84	Syntectonic	79.74469	13.06953	0.999883	69219	3503
R-11	Reinsdyrflya	13.9 ± 1.1	60	Migmatite	79.77957	13.08745	0.999765	60690	3811
R-12	Reinsdyrflya	13.9 ± 1.0	51	Syntectonic granite, gneissic	79.79582	13.35234	1.0	60085	3169
Mus-1	Mushamna	13.4 ± 1.0	39	Syntectonic, granite, gneissic	79.69184	14.28835	0.997564	57266	2964
Mus-2	Mushamna	34.6 ± 2.3	4	Syntectonic, light grey granite	79.68765	14.24290	0.999765	141421	6394
Kaf-1	Kaffitoppen	21.7 ± 1.4	836	Migmatite with pink plagioclase	79.46404	11.39372	0.988639	202352	8729
GraB	Granitten shoulder	44.5 ± 2.6	885	Hornemantoppen granite	79.54108	11.73848	0.997329	439974	13222
Reuy-1	Reuschhalvøya	11.7 ± 0.8	300	Syntectonic granite	79.63572	11.06336	0.999765	66191	3419
Carr-1	Carrfjellet, Buchananhalvøya	16.1 ± 1.8	110	Migmatite, very small grains	79.69622	12.15835	0.999730	74504	7750
Blom 1	Krossfjordflya	13.9 ± 1.0	19	Grey granite/migmatite	79.07100	11.67244	0.999672	58671	3032
Fall-1	Fallieresfjella	12.3 ± 0.9	227	Syntectonic, late tectonic granite	79.22097	12.02847	0.998570	64560	3467
Fall-2	Fallieresfjella	91.8 ± 5.3	210	Syntectonic granite	79.21951	12.02225	0.998726	465253	13979
Trong-1	Trongdalen	13.7 ± 1.0	169	Grey granite	79.18211	11.62969	0.999688	68218	3524
Trong-3	Trongdalen	30.9 ± 2.0	151	Syntectonic, late tectonic granite	79.17486	11.61175	0.999503	150391	6350
Flytt-22	Camp Zoe	18.1 ± 1.2	124	Migmatite with biotite	79.19385	11.96201	0.997469	85153	4164
Flytt-25	Camp Zoe	14.6 ± 1.0	32	Syntectonic, light grey granite	79.18087	11.87985	0.969705	60936	3092
Flak-1	Flakbreen, Camp Zoe	16.6 ± 1.1	162	Gneiss with biotite	79.19385	11.96201	0.999395	81485	3871
Flakstor	Flakbreen, Camp Zoe	16.8 ± 1.4	217	Gneiss	79.19140	12.00091	0.999095	87102	5747
Langskipet	Langskipet	24.8 ± 1.6	611	Gneiss	79.23881	11.81391	0.998611	189822	7612
Bedrock									
Gran-1	Granitten	39.5 ± 2.5	998	Hornemantoppen granite	79.54503	11.75530	0.992375	426354	17388
Gran-2	Granitten	81.0 ± 5.4	1079	Hornemantoppen granite	79.54754	11.75379	1.0	937171	40666
Gran-3	Granitten	57.9 ± 3.3	1075	Hornemantoppen granite	79.55667	11.76556	0.998547	670250	20126
Gran-4	Granitten	2.8 ± 0.2	998	Hornemantoppen granite	79.55642	11.77253	0.978592	30176	1859
Gran-5	Granitten	3.4 ± 0.4	998	Hornemantoppen granite	79.55642	11.77253	0.978592	36770	3379
Bjo	Aurivilliusfjellet	122.7 ± 8.2	878	Hornemantoppen granite	79.35605	11.49671	0.997446	1171171	50717
Carr T	Carfjellet, Buchananhalvøya	24.0 ± 1.6	80	Devonian conglomerate	79.70349	12.13153	0.999765	107172	5076
Jäd-1	Jäderinfjellet	17.2 ± 1.2	893	Migmatite	79.58522	11.94631	0.997329	170662	8395
Jäd-3	Jäderinfjellet	37.0 ± 2.1	1031	Migmatite	79.58687	11.95824	0.975957	405253	12177
Jäd-4	Jäderinfjellet	188.8 ± 12.0	1150	Migmatite	79.58897	11.97417	0.997564	2256862	83813
Horn-2	Hornemantoppen	118.4 ± 7.3	1094	Hornemantoppen granite	79.57678	11.72781	0.977301	1373461	49752
Horn-4	Hornemantoppen	70.8 ± 4.4	1026	Hornemantoppen granite	79.57253	11.73333	0.992492	778270	29899
Kjoek-2	Kjøkkensjefen, Losvikfjella	21.7 ± 2.3	1028	Syntectonic granite	79.52517	11.55561	0.5	124502	11610
Kjoek-3	Kjøkkensjefen, Losvikfjella	76.8 ± 4.4	956	Syntectonic granite	79.52492	11.54308	0.998547	872973	26216
Kjoek-4	Kjøkkensjefen, Losvikfjella	121.7 ± 10.3	934	Syntectonic granite	79.52428	11.54478	0.988639	1212372	80524
Mun-1	Munken	1.9 ± 0.2	893	Migmatite, schist	79.45321	11.97527	0.934292	17740	1610
Mun-2	Munken	22.1 ± 1.3	1043	Migmatite	79.45162	11.98679	0.975839	268645	8358
Mun-topp	Munken	19.6 ± 1.3	1190	Migmatite	79.44990	11.99360	0.999647	253266	11431
Muh-1	Munkehetta	16.1 ± 1.0	864	Migmatite	79.43601	11.96654	0.996346	170774	7042
Nisse-4	Nissenfjella	13.7 ± 0.8	455	Banded garnet-biotite gneiss	79.40365	11.03797	0.997564	99385	3520
Weg-2	Wegenerfjellet	3.5 ± 0.3	860	Migmatite	79.45558	11.76186	0.979810	36775	2312
Kaf-2	Kaffitoppen	41.3 ± 2.4	924	Migmatite with pink plagioclase	79.46647	11.38906	0.993593	457825	13762
AtgSum	Atgeiren	203.6 ± 12.1	933	Migmatite	79.48136	11.17835	0.989622	1987022	59632
Konge	Kongen	178.8 ± 10.6	1458	Syntectonic granite	79.29134	12.47574	0.999729	2779011	83385
Konge-2	Kongen	182.8 ± 10.8	1457	Syntectonic granite	79.29138	12.47584	0.998143	2836380	85104

Scaling scheme for age calculation: Lal (1991)/Stone (2000). Ages are adjusted to the regional production rate (Fenton et al., 2011). All boulders are <1.5 m high, except Lanskipet (Fig. 9g). For local lithology at boulder sites see Fig. 6.

Elevation flag, std; Sample thicknesses (cm), 5; Sample densities, 2.65; Erosion rates (cm/yr⁻¹), 0; ¹⁰Be standard, S2007N or 07KNSTD; ²⁶Al not measured.

Bockfjorden, a tributary fjord to Woodfjorden (Fig. 1), took place 10.9 cal ka BP (Salvigsen and Høgvard, 2005).

In the inner shelf and outer fjord mouth of Kongsfjorden there are several radiocarbon ages that constrain deglaciation. These are summarized and calibrated in Hormes et al. (submitted for publication). The eight ages that constrain deglaciation, six of which are basal ages from marine sediment cores, one of which is from a stratigraphic section on land, and one of which is from the marine limit on Brøggerhalvøya (directly south of Kongsfjorden), average 14.0 ± 0.9 cal ka BP. This deglaciation age of Kongsfjorden of ~ 14 ka is similar to our suggested ^{10}Be age for the deglaciation of the coastal areas surrounding NWS, including Mitrahøya, directly north of Kongsfjorden.

6.1.5. Early thinning, later retreat

Based on these data, it appears that retreat from the coastal areas surrounding the NWS occurred later than thinning in the central NWS mountains. One possibility is that the onset of frontal retreat indeed occurred earlier on the continental shelves, and that the ice margin did not retreat through our field areas until 14–16 ka. On the other hand, there is evidence that glacier retreat off the shelves and in the deep outer troughs occurs rapidly, and thus, it is possible that retreat off the shelves occurred after initial thinning is recorded in central NWS. Indeed, Jessen et al. (2010) noted that grounded ice on the western shelf edge of Svalbard started to retreat after ~ 20.5 ka, and on the outer northern shelf of Nordaustlandet, retreat started after 15.9 ka (Hormes et al., submitted for publication). Regardless, thinning this early during the LW is somewhat surprising, as it precedes the global rise in CO_2 and warming recorded in Antarctica ~ 19 ka (e.g., Shakun et al., 2012) and the more typical end of the LGM of the Northern Hemisphere ice sheets ~ 20 ka (e.g., Clark et al., 2009). If true, it remains unknown why the SBSIS would have thinned before significantly retreating. It may have to do with changing climatic regime or ice sheet geometry and/or basal conditions as the SBSIS evolved through the LW glaciation.

6.2. Thickness of the Late Weichselian ice sheet

We use the ^{10}Be ages of high-elevation erratic boulders to constrain the thickness of the ice dome during the LW. The ^{10}Be ages of summit bedrock also provide insight in the presence/absence of summit ice cover and basal conditions.

The three boulders in central NWS (Ovo-3, -4; Kaf-1; ranging from 18.3 ± 1.3 to 21.7 ± 1.4 ka) suggest that ice was >250 – 300 m thicker in this area during LW than today (Figs. 7 and 8). The erratic on Langskipet at 611 m a.s.l., which rises above 300-m-deep fjords (Möller and Lilliehöökfjorden) suggests an LW ice thickness of >900 m there (Fig. 9). The altitudinal position of the erratic Reuy-1 (11.7 ± 0.8 ka) at Reuschhalvøya (Fig. 1) is within the LW ice–surface profile projected from Amsterdamøya and Danskøya by Landvik et al. (2003).

The ^{10}Be ages from all bedrock of summit peaks pre-date the LW. Additionally, in general all the summit samples are older than samples collected at lower elevations. For example, the two bedrock ^{10}Be ages from the summit of Kongen (1458 m a.s.l.; 178.8 ± 10.6 and 182.8 ± 10.8 ka; Fig. 10) suggest that warm-based, erosive ice did not cover the highest peak in the area during the LW. Paired ^{10}Be and ^{26}Al data from Gjermundsen et al. (submitted for publication) indicate that summits in NWS have been repeatedly covered by cold-based, non-erosive ice during the Quaternary, likely during all maximum glacial phases. The prevalent burial detected by the paired isotopes is consistent with (but does not necessitate) peaks being covered by cold-based ice during LW. Ice covering Kongen would imply an ice sheet with a local surface elevation of up to 900 m thicker than at present (Fig. 10).

Our finding of a LW-age erratic high on Langskipet may be indicative that the summit of Kongen was possibly covered by ice in the early part of LW. If so, this would be contrary to Landvik et al. (2003), who suggested that LW ice was confined to the fjords, sounds, and coastal areas of northwestern most Spitsbergen. Could the highest peaks of NWS be ice covered while the summits of Amsterdamøya and Danskøya remained ice free? Hormes et al. (2011) suggested that the warm-based part of the ice sheet during the LW on Nordaustlandet (Fig. 1) was confined to the fjords and lowlands below 200–230 m a.s.l., with cold-based ice covering higher-elevation terrain. More recently, Landvik et al. (2013) suggest that during maximum LW glaciation, mountains >473 m a.s.l. on Prins Karls Forland (Fig. 1) were covered by ice, and possibly mountains >313 m a.s.l. on Mitrahøya were covered by ice. This would imply relatively thick ice over NWS and also supports the possibility that Kongen could have been covered.

Taking Landvik et al.'s (2013) conclusion about the LW ice sheet elevation on Prins Karls Forland, and that the ice was flowing from Spitsbergen westwards to Prins Karls Forland, thickness of ice in the NWS can be estimated. Assuming an ice surface slope of 20–40 m/km (Landvik et al., 2003) indicates an ice surface elevation of ~ 1100 – 1700 m a.s.l. at Engelskbukta (Fig. 1), consistent with ice over Langskipet in Krossfjorden at 611 m a.s.l., and potentially over Kongen at 1450 m a.s.l. Taking another approach to estimate the ice surface gradient itself, we consider the Ovo-3 and -4 sites on Aurivilliusfjellet (Fig. 7). Between these sites and the shelf edge, at the reconstructed terminus of LW, ice would yield an average gradient of 23 m/km, consistent with Landvik et al. (2003).

The ^{10}Be ages of the two samples on Kaffitoppen, one erratic boulder on its southeast ridge (Kaf-1 at 836 m a.s.l.; 21.7 ± 1.4 ka; Fig. 8) and the bedrock sample on the northeast ridge (Kaf-2 at 924 m a.s.l.; 41.3 ± 2.4 ka) potentially reveal an ice surface elevation during the LW between 836 and 924 m a.s.l. This mountain is close to today's coast and more distal to the centre of our proposed ice dome (Fig. 6). However, the age of sample Kaf-2 might simply indicate that the erosion during LW was minimal at the site, leaving pre-LW accumulated isotopes in the bedrock and that the summit actually was covered and that Kaf-1 represents a period during the retreat.

Even closer to the western coastline is Atgeiren at 933 m a.s.l. (AtgSum, 203.6 ± 12.1 ka; Fig. 4). The antiquity of the summit relative to the apparent ^{10}Be ages of the other summits throughout NWS could be due to its location more distal to the centre of our proposed ice sheet dome (Fig. 6). This would be in agreement with the conclusions of Briner et al. (2006) who noted that bedrock surfaces distal to the ice sheet are generally older than those in inter-fjords and valleys farther inland. Measuring ^{26}Al from the AtgSum sample might indicate whether this mountain has been covered with ice for a shorter duration than the more central peaks in NWS (Gjermundsen et al., submitted for publication), and $^{14}\text{C}/^{10}\text{Be}$ ratios of the summit sample could reveal whether it was covered during LW.

If we imply the same reasoning about the ice sheet elevation as we did in Smeerenburgfjorden and assume that the ice sheet surface had a constant gradient from Langskipet to today's ice shed of 23 m/km, we get an ice surface elevation over Staxrudfonna of 1350 m a.s.l. This would cover the highest peak in the area, Munken (1205 m a.s.l.) However, the dynamics of the ice dome were possibly complex, being controlled by today's topography without a constant slope gradient, but rather a shifting one between localities.

6.3. Late Weichselian ice dome configuration and characteristics

6.3.1. Ice dome configuration

A local ice dome occupying the NWS during LW was first proposed by Salvigsen (1979), who suggested a local ice

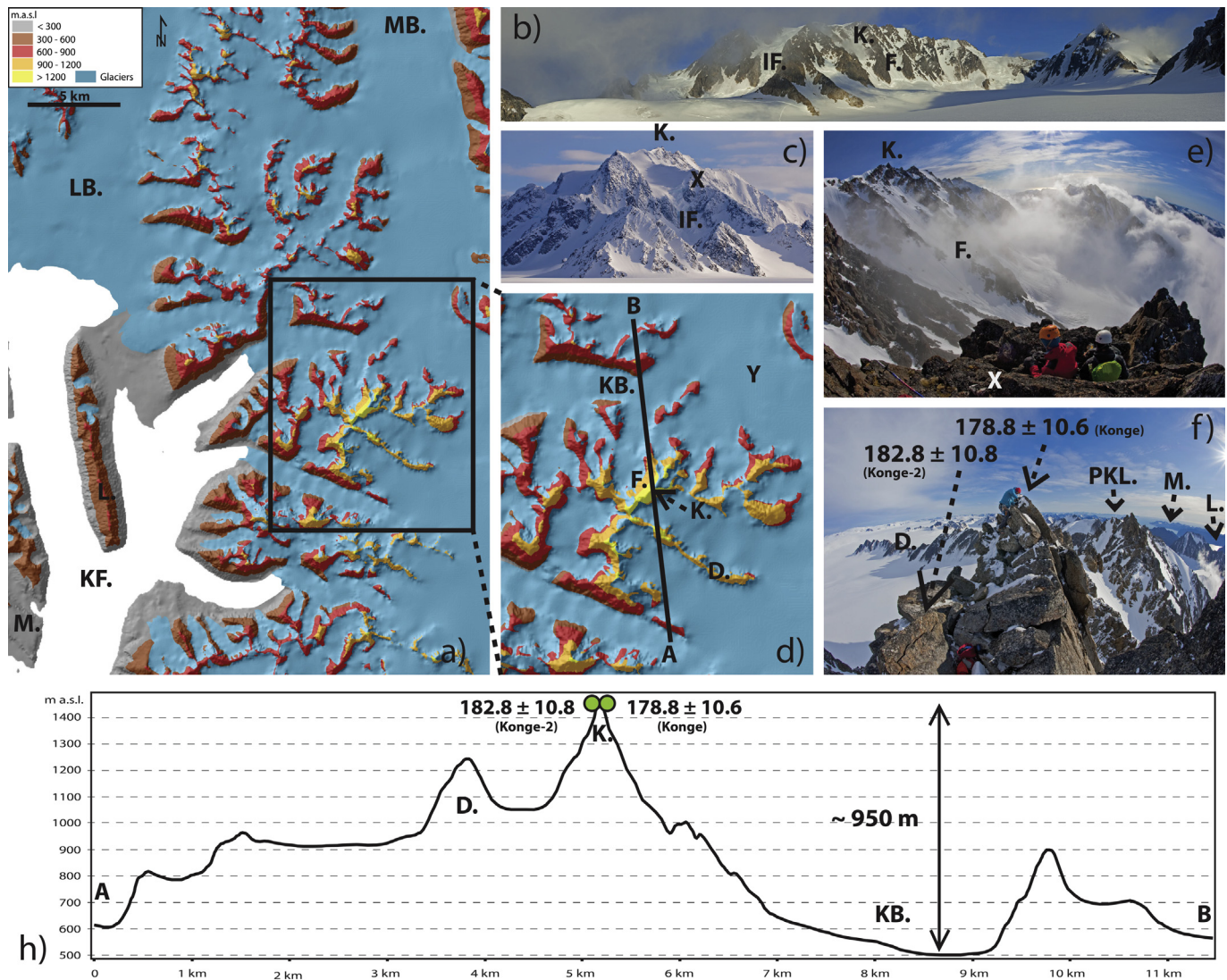


Fig. 10. Kongen, the highest mountain in Northwest Spitsbergen (1458 m a.s.l.). a) Overview of the area, b) the long summit ridge of Kongen seen from northwest, c) Kongen seen from position Y in d) (north), d) close up view of the area showing the location of the profile given in h), e) the summit of Kongen seen from the northwest ridge (position X in fig. c)), f) the very summit of Kongen, showing the sampling sites, h) profile through Kongen as given in d). The arrows in the profile indicate the surface lowering which might have taken place since LW if Kongen was covered at that time. Abbreviations from left to right: M = Mitrahallvøya, KF = Krossfjorden, L = Lanskipet, LB = Lillehöökreen, MB = Monacobreen, KB = Kollerbreen, F = northwest face of Kongen, K = Kongen, IF = Icefall, D = Drygalskikammen.

centre between Smeerenburgfjorden and Liefdefjorden based on provenance of erratics in outlying areas. However, [Salvigsen \(1979\)](#) also noted the tilt of the Holocene strandlines in this area, rising from the head of Liefdefjorden to the mouth of Liefdefjorden. With a local ice dome configuration, one would expect isostatic uplift to be greatest near the ice centre. Rather, the strandline pattern seems to be dominated by the large SBSIS with the area of maximum emergence farther east. This pattern might indicate that the presence of the local ice dome was short-lived (e.g., a feature of the latter stages of LW glaciation) or the ice was thinner in this area than our data suggest. [Long et al. \(2012\)](#) used radiocarbon dating of marine shells on raised beaches on central Spitsbergen to reconstruct changes in relative sea level and concluded that the ice load from local ice domes were too small to modify the regional pattern from the SBSIS. [Salvigsen et al. \(1995\)](#) used glacial striae and other ice movement indicators to identify LW ice movement in eastern Svalbard and the northern Barents Sea. They documented the change in ice flow direction during the LW; first there was ice flow from the east (regional ice cover with the centre over Barents Sea),

and then later ice flow from west to east (local ice cover). Such change in ice flow direction is reflected in the raised beach terraces, and underlines the difficulty of recognizing local pattern in NWS.

Based on our lithological investigations of the erratic boulders on Reinsdyrflya, we suggest ice flow onto Reinsdyrflya from the central NWS through Liefdefjorden ([Fig. 6](#)). The area east of Vonbreen (at the head of Woodfjorden) is dominated by Devonian sandstone and shale ([Fig. 6](#)). The lack of sedimentary boulders on Reinsdyrflya indicates that the ice that flowed through Woodfjorden did not cross Reinsdyrflya but was confined to the fjord ([Fig. 6](#)). The only exception to the observation of this was one erratic conglomerate. This erratic, however, likely originated from the inner part of Liefdefjorden. This is further supported by striae on Reinsdyrflya observed by [Salvigsen and Österholm \(1982\)](#) indicating that the last ice movement came from the southwest. They observed Hornemantoppen Granite erratics on Reinsdyrflya, but no Hornemantoppen Granite erratics were found east of Woodfjorden. [Salvigsen and Österholm \(1982\)](#) also suggested that the deglaciation of the eastern islands in Liefdefjorden took place



Fig. 11. Panoramic photo of the terrain south of Camp Zoe in Krossfjorden, showing our identified upper boundary of glacier drift. This drift limit is interpreted as a thermal regime boundary rather than an ice margin.

earlier compared to the ones farther west. Their observations further support the idea of a local ice dome in central NWS during the LW and that all ice on Reinsdyrflya came from the west and southwest. The syntectonic granite erratics found on Reinsdyrflya (Fig. 6; Table 1) have been transported over a long distance from sources in central NWS. Seligerbreen and Monacobreen are the most likely former locations of ice streams (Fig. 6). The fact that Hornmantoppen Granites are not found in Krossfjorden would suggest that the central NWS ice dome mainly drained to the north, east and west, and that the ice stream draining through Krossfjorden was mainly fed by glaciers from the northeast, such as Kollerbreen, Supanbreen and Isachsenfonna (Fig. 6).

The lithology of Reuy-1 (11.7 ± 0.8 ka; syntectonic granite) at Reuschhalvøya (Fig. 1) indicates a drainage system from the east/southeast, where Smeerenburgbreen is located at present (Fig. 1). Reuy-2 was not dated but is a Hornemantoppen Granite and indicates a westward flow of ice streams from the Hornemantoppen region. Our two samples from Aurivilliusfjellet (Ovo-3 and Ovo-4; 20.1 ± 1.6 ka and 18.3 ± 1.3 ka, respectively) are most likely deposited by a northwestward flowing ice through Hans Henrikbreen with provenance regions southeast and east of Aurivilliusfjellet (Fig. 7). Kaf-1 (21.7 ± 1.4 ka), is a boulder perched on a narrow ridge and clearly not a rock fallen from the mountain top (Fig. 8). The older ^{10}Be age of the bedrock ~ 25 m higher (41.3 ± 2.4 ka) shows that young erratics can be perched atop old bedrock (cf. Briner et al., 2003). This boulder must have been transported from another provenance of migmatite. From the gneissic origin of the Langskipet sample we interpret ice flow from the north or northeast along Lillehöökreen or Kollerbreen (Figs. 1 and 9).

Our reconstruction supports the hypothesis of a complex multi-dome ice-sheet configuration over Svalbard and the Barents Sea during the LW, with numerous drainage basins feeding fast-flowing ice streams, separated by slow-flowing, possibly cold-based ice, in inter-ice-stream areas (Landvik et al., 2005; Ottesen et al., 2007; Ottesen and Dowdeswell, 2009; Alexanderson et al., 2011; Hormes et al., 2011; Landvik et al., 2013). Consistent with this, Dowdeswell et al. (2010) concluded that a major ice dome was located on easternmost Spitsbergen or southern Hinlopen Strait during LW.

6.3.2. Basal ice sheet characteristics

The well-preserved raised beaches on Reinsdyrflya, combined with the lack of moraine deposits (Salvigsen and Österholm, 1982) lead us to suggest that the ice covering Reinsdyrflya possibly was cold-based, leaving the pre-LW landscape intact. It is likely that Reinsdyrflya resided as an inter ice-stream area with fast flowing ice restricted to Liefdefjorden and Woodfjorden. On the eastern side of Krossfjorden, near Camp Zoe (Fig. 1), a glacier drift limit from present sea level up to ~ 120 m a.s.l. consisting of migmatite, granite, gneiss, and conglomerate boulders, clearly different from the local bedrock of mica schist, potentially delimits a thermal boundary of the ice (Fig. 11). A similar drift limit has been identified

in nearby Kongsfjorden at an elevation of ~ 35 m (Houmark-Nielsen and Funder, 1999). In any case the drift limit in Krossfjorden suggests that Mitrahallvøya belonged to an inter-ice stream area during LW. Because some of the erratics that yield LW ages are from higher elevations, we suggest that the drift limit boundary represents a thermal boundary within the LW ice sheet. In this scenario, ice below the drift limit boundary would have been warm-based and erosive, and the ice above, including on Langskipet, was perhaps cold-based for some or all of the LW glaciation. Such a depiction of fast-flowing ice restricted to the fjord axes and less active ice on high-elevation areas and distal coastal lowlands, like at Reinsdyrflya, is becoming a commonly accepted reconstruction on Svalbard (e.g., Landvik et al., 2005) and elsewhere (e.g., Briner et al., 2005).

The vertical transects in central NWS may also provide some insight into the ice sheet's thermal boundary. Our summit transects show a trend (Table 1) of the oldest ages at the highest elevations and decreasing age towards lower elevations. This alone does not prove that the ice did not cover the highest peaks. It could be interpreted that the ice became more erosive at lower elevations, removing more of the pre-LW ^{10}Be concentration. For example, our lowermost bedrock sample from Jäderinfjellet (Jäd-1; 893 m a.s.l.) is from just above today's glacier surface (~ 700 m a.s.l.) and given the age (17.2 ± 1.2 ka) it falls within the timeframe of our deglaciation ages (Fig. 5). Thus, we suggest it represents the deglaciation at this location and possibly indicates the presence of warm-based, erosive ice at this location during the LW. Regardless, we cannot rule out that the peaks remained ice free during the LW, but the pattern of ^{10}Be ages in our profiles is consistent with accumulating evidence that this is the expected pattern in polythermal ice sheet landscapes (Landvik et al., 2005; Sugden et al., 2005; Briner et al., 2006; Goehring et al., 2008).

7. Conclusions

During the Late Weichselian, central NWS was covered by a local ice dome that drained radially, but transported Hornemantoppen granite to the east, north and west. Three high-elevation erratic boulders in central NWS indicate that the centre of this local ice dome was >300 m higher than the present ice surface. One erratic boulder on the summit ridge of Langskipet at 600 m a.s.l. in Krossfjorden suggests that the ice in this fjord had a thickness of >900 m (fjord depth ~ 300 m) during the LW. Estimations of interior ice sheet thickness based on the elevation of the Langskipet sample and possible ice sheet surface slope suggests that this ice dome in central NWS might have reached elevations of >1350 m a.s.l. during the LW. Despite the presence of a thick, local ice dome over NWS, raised beach terraces in the area do not show evidence of a local ice dome, indicating that the pattern of former shorelines is dominated by the larger SBSIS centre to the east.

Several ^{10}Be ages from bedrock samples from vertical transects on mountains in the area generally yield the oldest ages at the

highest elevations. This indicates that the ice at lower elevations was more erosive and that the summits in the area either were ice-free during LW or covered with cold-based non-erosive ice. Summit samples from Atgeiren, Kongen and Jäderinfjellet all give very old exposure ages of ~200 ka, indicating that these summits either have been exposed during the last few glacial cycles or covered by cold-based non-erosive ice.

The ^{10}Be ages from seven erratic boulders on Reinsdyrflya indicate ice cover over the entire Reinsdyrflya during LW, and complete deglaciation prior to the Holocene. Lack of moraine deposits, but the preserved beach terraces, suggest that the ice covering this peninsula possibly was cold-based and that Reinsdyrflya was part of an inter ice-stream area covered by slow-flowing ice, as opposed to the adjacent fjord, which possibly was filled by a fast-flowing ice stream. The LW ice flow through Woodfjorden and Bockfjorden do not seem to have crossed Reinsdyrflya. A glacier drift boundary at ~120 m a.s.l. in Krossfjorden suggests that the ice above this elevation likely was cold-based, confining warm-based ice here to the lowest elevations along the fjords.

The ^{10}Be ages from our high-elevation erratics indicate an earlier onset of ice sheet thinning (25–20 ka) than previously suggested. Despite the relatively early onset of thinning, our distal erratics point towards a later deglaciation of the distal areas, suggesting that thinning preceded ice margin retreat. Changing ice sheet dynamics and basal characteristics through the LW may have led to this pattern.

Acknowledgements

Economical support for field work was provided by internal UNIS funding, along with Arctic Field Grants from SSF to Endre F.G. Additionally, some funds for field work were provided by NAROM/Birgit Strømsholm and Jan Christensens Endowment. Cosmogenic surface exposure dating was supported through internal UNIS funding to Anne H. Helge Kåsin, Tobias Hipp, Bjørn André Skjæret, Trygve Snøtun, Jakob Fjellanger, Carl Petter Nielsen and Halvor Dannevig are thanked for their enormous effort and invaluable help during all the field campaigns. A special thanks to Jakob Fjellanger who discovered the erratics on Langskipet on our field campaign in Krossfjorden summer 2010. Heavy logistic support was provided by the French German base AWIPEV, some logistical supports were provided by UNIS. We thank all our sponsors (see Icebound.no). Thin sections for some of our samples were made at the University of Tromsø by Trine Dahl. Bathymetric information for constructing the subsea profile in Fig. 9 was provided by The Norwegian Mapping Authorities Sea, (Statens Kartverk Sjø) with authorization nr 08/620. We thank the reviewers Henriette Linge and Robert Ackert for their very constructive comments improving this manuscript.

References

Akçar, N., 2006. Paleoglacial Records from the Black Sea Area of Turkey Field and Dating Evidence. Geological Institute. PhD thesis. Bern University, Bern.

Akçar, N., Ivy-Ochs, S., Kubik, P.W., Schluchter, C., 2011. Post-depositional impacts on 'Findlinge' (erratic boulders) and their implications for surface-exposure dating. *Swiss Journal of Geosciences* 104, 445–453.

Alexanderson, H., Landvik, J.Y., Ryen, H.T., 2011. Chronology and styles of glaciation in an inter-fjord setting, northwestern Svalbard. *Boreas* 40, 175–197.

Andersen, B.G., 1981. Late Weichselian ice sheets in Eurasia and Greenland. In: Denton, G.H.H.T.J. (Ed.), *The Last Great Ice Sheets*. John Wiley & Sons, New York, pp. 1–65.

Andersson, T., Forman, S.L., Ingolfsson, O., Manley, W.F., 1999. Late Quaternary environmental history of central Prins Karls Forland, western Svalbard. *Boreas* 28, 292–307.

Balco, G., Stone, J.O., Lifton, N.A., Dunai, T.J., 2008. A complete and easily accessible means of calculating surface exposure ages or erosion rates from ^{10}Be and ^{26}Al measurements. *Quaternary Geochronology* 3, 174–195.

Boulton, G.S., 1979. Glacial history of the Spitsbergen archipelago and the problem of a Barents Shelf ice sheet. *Boreas* 8, 31–57.

Boulton, G.S., Baldwin, C.T., Peacock, J.D., McCabe, A.M., Miller, G.H., Jarvis, J., Horsefield, B., Worsley, P., Eyles, N., Chroston, P.N., Day, T.E., Gibbard, P., Hare, P.E., von Brunn, V., 1982. A glacioisostatic facies model and amino acid stratigraphy for late Quaternary events in Spitsbergen and the Arctic. *Nature* 298, 437–441.

Briner, J.P., Miller, G.H., Davis, P.T., Bierman, P.R., Caffee, M., 2003. Last glacial maximum ice sheet dynamics in Arctic Canada inferred from young erratics perched on ancient tors. *Quaternary Science Reviews* 22, 437–444.

Briner, J.P., Miller, G.H., Davis, P.T., Finkel, R.C., 2005. Cosmogenic exposure dating in arctic glacial landscapes: Implications for the glacial history of northeastern Baffin Island, Arctic Canada. *Canadian Journal of Earth Sciences* 42, 67–84.

Briner, J.P., Miller, G.H., Thompson Davis, P., Finkel, R.C., 2006. Cosmogenic radionuclides from fiord landscapes support differential erosion by overriding ice sheets. *GSA Bulletin* 118, 406–420.

Brückner, H., Schellmann, G., 2003. Late Pleistocene and holocene shorelines of Andreeland, Spitsbergen (Svalbard) – geomorphological evidence and palaeo-oceanographic significance. *Journal of Coastal Research* 19, 971–982.

Brückner, H., Schellmann, G., van der Borg, K., 2002. Uplifted beach ridges in northern Spitsbergen as indicators for glacio-isostasy and palaeo-oceanography. *Zeitschrift für Geomorphologie*, N.F 46, 309–336.

Clark, P.U., Dyke, A.S., Shakun, J.D., Carlson, A.E., Clark, J., Wohlfarth, B., Mitrovica, J.X., Hostetler, S.W., McCabe, A.M., 2009. The last glacial maximum. *Science* 325, 710–714.

Codilean, A.T., 2006. Calculation of the cosmogenic nuclide production topographic shielding scaling factor for large areas using DEMs. *Earth Surface Processes and Landforms* 31, 785–794.

Dallmann, W.K., Ohta, Y., Elvevold, S., Blomeier, D., 2002. Bedrock Map of Svalbard an Jany Mayen. Temakart No. 33. Norwegian Polar Institute.

Dowdeswell, J.A., Hogan, K.A., Evans, J., Noormets, R., O'Coiffaigh, C., Ottesen, D., 2010. Past ice-sheet flow east of Svalbard inferred from streamlined subglacial landforms. *Geology* 38, 163–166.

Dunne, J., Elmore, D., Muzikar, P., 1999. Scaling factors for the rates of production of cosmogenic nuclides for geometric shielding and attenuation at depth on slope surfaces. *Geomorphology* 27, 3–11.

Elverhøi, A., Anders, E.S., Dokken, T., Hebblen, D., Spielhagen, R., Svendsen, J., Sørflaten, M., Rørnes, A., Hald, M., Forsberg, C.S., 1995. The growth and decay of the Late Weichselian ice sheet in western Svalbard and adjacent areas based on provenance studies of marine sediments. *Quaternary Research* 44, 303–316.

Elverhøi, A., Dowdeswell, J.A., Funder, S., Mangerud, J., Stein, R., 1998. Glacial and oceanic history of the Polar North Atlantic margins: an overview. *Quaternary Science Reviews* 17, 1–10.

Fenton, C.R., Hermanns, R.L., Blikra, L.H., Kubik, P.W., Bryant, C., Niedermann, S., Meixner, A., Goethals, M.M., 2011. Regional ^{10}Be production rate calibration for the past 12 ka deduced from the radiocarbon-dated Grøtlandsura and Russenes rock avalanches at 69°N, Norway. *Quaternary Geochronology* 6, 437–452.

Forman, S.L., 1990. Post-glacial relative sea-level history of northwestern Spitsbergen, Svalbard. *Geological Society of America Bulletin* 102, 1580–1590.

Forman, S.L., Lubinski, D.J., Ingolfsson, O., Zeeberg, J.J., Snyder, J.A., Siegert, M.J., Matishov, G.G., 2004. A review of postglacial emergence on Svalbard, Franz Josef Land and Novaya Zemlya, northern Eurasia. *Quaternary Science Reviews* 23, 1391–1434.

Forman, S.L., Miller, G.H., 1984. Time-dependent soil morphologies and pedogenic processes on raised beaches, Brøggerhalvøya, Spitsbergen, Svalbard Archipelago. *Arctic and Alpine Research* 16, 381–394.

Gee, D.G., Fossen, H., Henriksen, N., Higgins, A.K., 2008. From the early Paleozoic platforms of Baltica and Laurentia to the Caledonide Orogen of Scandinavia and Greenland. *Journal of International Geoscience* 31, 44–51.

Gjermundsen, E.F., Briner, J., Akçar, N., Kubik, P., Salvigsen, O., Hormes, A. Arctic Alpine Topography Minimally Carved during Repeated Quaternary Glaciation, submitted for publication.

Goehring, B.M., Brook, E.J., Linge, H., Ralsbeck, G.M., Yiou, F., 2008. Beryllium-10 exposure ages of erratic boulders in southern Norway and implications for the history of the Fennoscandian Ice Sheet. *Quaternary Science Reviews* 27, 320–336.

Grosswald, M.G., Hughes, T.J., 1995. Paleoglacialogy grand unsolved problem. *Journal of Glaciology* 41, 313–332.

Hagen, J.O., Liestøl, O., Roland, E., Jørgensen, T., 1993. Glacier atlas of Svalbard and Jan Mayen. *Norsk Polarinstittutt Meddelelser* 129, 141.

Hogan, K.A., Dowdeswell, J.A., Noormets, R., Evans, J., O'Coiffaigh, C., 2010. Evidence for full-glacial flow and retreat of the Late Weichselian Ice Sheet from the waters around Kong Karls Land, eastern Svalbard. *Quaternary Science Reviews* 29, 3563–3582.

Hormes, A., Akçar, N., Kubik, P.W., 2011. Cosmogenic radionuclide dating indicates ice-sheet configuration during MIS 2 on Nordaustlandet, Svalbard. *Boreas* 40, 636–649.

Hormes, A., Gjermundsen, E.F., Rasmussen, T.L. From mountain top to the deep sea – deglaciation in 4D of the northwestern Barents Sea Ice sheet. *Quaternary Science Reviews*, submitted for publication.

Houmark-Nielsen, M., Funder, S., 1999. Pleistocene stratigraphy of Kongsfjordhallet, Spitsbergen, Svalbard. *Polar Research* 18, 39–49.

Ivy-Ochs, S., Schlüchter, C., Kubik, P.W., Synal, H.-A., Beer, J., Kerschner, H., 1996. The exposure age of an Egesen moraine at Julier Pass, Switzerland, measured with the cosmogenic radionuclides ^{10}Be , ^{26}Al and ^{36}Cl . *Eclogae geologicae Helveticae* 89 (3), 1049–1063.

- Jessen, S.P., Rasmussen, T.L., Nielsen, T., Solheim, A., 2010. A new Late Weichselian and Holocene marine chronology for the western Svalbard slope 30,000–0. cal years BP. *Quaternary Science Reviews* 29, 1301–1312.
- Knies, J., Matthiessen, J., Vogt, C., Laberg, J.S., Hjelstuen, B.O., Smelror, M., Larsen, E., Andreassen, K., Eidvin, T., Vorren, T.O., 2009. The Plio-Pleistocene glaciation of the Barents Sea-Svalbard region: a new model based on revised chronostratigraphy. *Quaternary Science Reviews* 28, 812–829.
- Kohl, C.P., Nishiizumi, K., 1992. Chemical isolation of quartz for measurement of in situ-produced cosmogenic nuclides. *Geochimica et Cosmochimica Acta* 56, 3583–3587.
- Kubik, P.W., Christl, M., 2010. ^{10}Be and ^{26}Al measurements at the Zürich 6 MV Tandem AMS facility. *Nuclear Instruments & Methods In Physics Research Section B* 268, 880–883.
- König, M., Nuth, C., Kohler, J., Moholdt, G., Pettersen, R., 2011. A Digital Glacier Database for Svalbard. GLIMS publication. Submitted for publication.
- Lal, D., 1991. Cosmic ray labeling of erosion surfaces: in-situ nuclide production rates and erosion models. *Earth and Planetary Science Letters* 104, 424–439.
- Landvik, J.Y., Bondevik, S., Elverhøi, A., Fjeldskaar, W., Mangerud, J., Salvigsen, O., Siegert, M.J., Svendsen, J.I., Vorren, T.O., 1998. The last glacial maximum of Svalbard and the Barents Sea area: ice sheet extent and configuration. *Quaternary Science Reviews* 17, 43–75.
- Landvik, J.Y., Brook, E.J., Gualtieri, L., Raisbeck, G., Salvigsen, O., Yiou, F., 2003. Northwest Svalbard during the last glaciation: ice-free areas existed. *Geology* 31, 905–908.
- Landvik, J.Y., Ingólfsson, O., Mienert, J., Lehman, S.J., Solheim, A., Elverhøi, A., Ottesen, D., 2005. Rethinking Late Weichselian ice-sheet dynamics in coastal NW Svalbard. *Boreas* 34, 7–24.
- Landvik, J., Brook, E.J., Gualtieri, L., Linge, H., Raisbeck, G., Salvigsen, O., Yiou, F., 2013. ^{10}Be exposure age constraints on the Late Weichselian ice sheet geometry and dynamics in inter ice-stream areas, western Svalbard. *Boreas* 42, 43–56.
- Lehman, S.J., 1989. Late Quaternary Glacial and Marine Paleoenvironments of Northwest Spitsbergen, Svalbard. University of Colorado, Boulder, p. 236.
- Li, Y.K., Harbor, J., Stroeven, A.P., Fabel, D., Kleman, J., Fink, D., Caffee, M., Elmore, D., 2005. Ice sheet erosion patterns in valley systems in northern Sweden investigated using cosmogenic nuclides. *Earth Surface Processes and Landforms* 30, 1039–1049.
- Long, A.J., Strzelecki, M.C., Lloyd, J.M., Bryant, C.L., 2012. Dating high Arctic Holocene relative sea level changes using juvenile articulated marine shells in raised beaches. *Quaternary Science Reviews* 48, 61–66.
- Mangerud, J., Bolstad, M., Elgersma, A., Helliksen, D., Landvik, J.Y., Lønne, I., Lycke, A.K., Salvigsen, O., Sandahl, T., Svendsen, J.I., 1992. Last glacial maximum on Spitsbergen, Svalbard. *Boreas* 38, 1–31.
- Mangerud, J., Dokken, T., Hebbeln, D., Heggen, B., Ingólfsson, O., Landvik, J.Y., Mejdahl, V., Svendsen, J.I., Vorren, T.O., 1998. Fluctuations of the Svalbard-Barents Sea Ice Sheet during the last 150 000 years. *Quaternary Science Reviews* 17, 11–22.
- Mangerud, J., Bondevik, S., Gulliksen, S., Hufthammer, K.A., Høisaeter, T., 2006. Marine ^{14}C reservoir ages for 19th century whales and molluscs from the North Atlantic. *Quaternary Science Reviews* 25, 3228–3245.
- Mangerud, J., Svendsen, J.I., 1992. The last interglacial-glacial period on Spitsbergen, Svalbard. *Quaternary Science Reviews* 11, 633–664.
- Masarik, J., Frank, M., Schäfer, J.M., Wieler, R., 2001. Correction of in situ cosmogenic nuclide production rate for geomagnetic field intensity variations during the past 800,000 years. *Geochimica et Cosmochimica Acta* 65, 2995–3003.
- Masarik, J., Reedy, R.C., 1995. Terrestrial cosmogenic-nuclide production systematics calculated from numerical simulations. *Earth and Planetary Science Letters* 136, 381–395.
- Nuth, C., Kohler, J., Aas, H.F., Brandt, O., Hagen, J.O., 2007. Glacier geometry and elevation changes on Svalbard (1936–90): a baseline dataset. *Annals of Glaciology* 46, 106–116.
- Ohta, Y., Larionov, A.N., Tebenkov, A.M., Lepvrier, C., Maluski, H., Lange, M., Hellebrandt, B., 2002. Single-zircon Pb-evaporation and Ar-40/Ar-39 dating of the metamorphic and granitic rocks in north-west Spitsbergen. *Polar Research* 21, 73–89.
- Ottesen, D., Dowdeswell, J.A., 2009. An inter-ice-stream glaciated margin: submarine landforms and a geomorphic model based on marine-geophysical data from Svalbard. *Geological Society of America Bulletin* 121 (11/12), 1647–1665. <http://gsabulletin.gsapubs.org/content/121/11-12/1647.short>.
- Ottesen, D., Dowdeswell, J.A., Landvik, J.Y., Mienert, J., 2007. Dynamics of the Late Weichselian ice sheet on Svalbard inferred from high-resolution sea-floor morphology. *Boreas*, 286–306.
- Phillips, W.M., Hall, A.M., Mottram, R., Fifield, L.K., Sugden, D.E., 2006. Cosmogenic Be-10 and Al-26 exposure ages of tors and erratics, Cairngorm Mountains, Scotland: timescales for the development of a classic landscape of selective linear glacial erosion. *Geomorphology* 73, 222–245.
- Salvigsen, O., 1979. The last deglaciation of Svalbard. *Boreas* 8, 229–231.
- Salvigsen, O., Adrielson, L., Hjort, C., Kelly, M., Landvik, J.Y., Ronnert, L., 1995. Dynamics of the last glaciation in eastern Svalbard inferred from glacier-movement indicators. *Polar Research* 14, 141–152.
- Salvigsen, O., Høgvard, K., 2005. Glacial history, Holocene shoreline displacement and palaeoclimate based on radiocarbon ages in the area of Bockfjorden, northwestern Spitsbergen, Svalbard. *Polar Research* 125, 15–24.
- Salvigsen, O., Österholm, H., 1982. Radiocarbon dated raised beaches and glacial history of the northern coast of Spitsbergen, Svalbard. *Polar Research* 1, 97–115.
- Schytt, V., Hoppe, G., Blake Jr., W., Grosswald, M.G., 1968. A preliminary report about the Stockholm University Svalbard Expedition 1966. The Extent of the Würm Glaciation in the European Arctic, vol. 79. International Association of Scientific Hydrology Publication, pp. 207–216.
- Shakun, J.D., Clark, P.U., He, F., Marcott, S.A., Mix, A.C., Liu, Z.Y., Otto-Bliesner, B., Schmittner, A., Bard, E., 2012. Global warming preceded by increasing carbon dioxide concentrations during the last deglaciation. *Nature* 484, 49–54.
- Siegert, M.J., Dowdeswell, J.A., Svendsen, J.I., Elverhøi, A., 2002. The Eurasian arctic during the last ice age. *American Scientist* 90, 32–39.
- Solheim, A., Andersen, E.S., Elverhøi, A., Fiedler, A., 1996. Late Cenozoic depositional history of the western Svalbard continental shelf, controlled by subsidence and climate. *Global and Planetary Change* 12, 135–148.
- Stone, J.O., 2000. Air pressure and cosmogenic isotope production. *Journal of Geophysical Research – Solid Earth* 105 (B10), 23753–23759.
- Stroeven, A.P., Fabel, D., Hattestrand, C., Harbor, J., 2002. A relict landscape in the centre of Fennoscandian glaciation: cosmogenic radionuclide evidence of tors preserved through multiple glacial cycles. *Geomorphology* 44, 145–154.
- Sugden, D.E., Balco, G., Cowdery, S.G., Stone, J.O., Sass, L.C., 2005. Selective glacial erosion and weathering zones in the coastal mountains of Marie Byrd Land, Antarctica. *Geomorphology* 67, 317–334.
- Sund, M., Eiken, T., Hagen, J.O., Kääb, A., 2009. Svalbard surge dynamics derived from geometric changes. *Annals of Glaciology* 50, 50–60.
- Svendsen, J.I., Alexanderson, H., Astakhov, V.I., Demidov, I., Dowdeswell, J.A., Funder, S., Gataullin, V., Henriksen, M., Hjort, C., Houmark-Nielsen, M., 2004. Late Quaternary ice sheet history of northern Eurasia. *Quaternary Science Reviews* 23, 1229–1271.
- Thiede, J., Winkler, A., Wolf-Welling, Eldholm, O., Myhre, A.M., Baumann, K.-H., Henrich, R., Stein, R., 1998. Late cenozoic history of the Polar North Atlantic: results from ocean drilling. *Quaternary Science Reviews* 17, 185–208.
- Troitsky, L., Punning, J.M., Hutt, G., Rajamae, R., 1979. Pleistocene glaciation chronology of Spitsbergen. *Boreas* 8, 401–407.
- Vorren, T.O., Landvik, J.Y., Andreassen, K., Laberg, J.S., 2010. Glacial history of the Barents sea region. In: Ehlers, J., Gibbard, P.L., Hughes, P.D. (Eds.), *Developments in Quaternary Science*. Elsevier, Amsterdam, pp. 361–372.